XV. PLASMA ELECTRONICS*

Prof. L. D. Smullin
Prof. H. A. Haus
Prof. A. Bers
Prof. D. J. Rose
Prof. T. H. Dupree
Prof. E. P. Gyftopoulos
Dr. G. Fiocco
Dr. K. Takaki
W. L. Brassert
H. Breindel
J. R. Cogdell
A. R. Cook
L. J. Donadieu
T. J. Fessenden
W. D. Getty
G. C. Hartmann
W. C. Homeyer
H. Y. Hsieh
A. J. Impink, Jr.
P. W. Jameson
L. E. Lidsky
D. L. Morse
A. Poeltinger
S. D. Rothleder
W. D. Rummler
A. J. Schneider
P. E. Serafim
P. S. Spangler
G. A. Stoops
G. C. Theodoridis
E. Thompson
J. S. Tulenko
S. Wilensky
J. N. Wilson

RESEARCH OBJECTIVES

1. Plasmas for Electrical Energy Conversion

During the coming year the work of this group will be concerned with the following problems:

Heating of a Plasma by Interaction with an Electron Beam. The experiments of W. Getty (reported in past QPR's) indicated that a powerful electron beam drifting through a plasma can excite intense oscillations in the system. In his experiments plasma electrons were excited to energies in excess of 100 ev, and the 10 kev beam electrons were scattered. This electron beam may be a useful device for heating a potential thermonuclear plasma.

In the coming year, we shall undertake the following theoretical work: 1) extend the analysis beyond its present quasistatic approximations to allow us to predict the behavior of systems with lateral dimensions $L \gg \lambda_p = c/f_p$; 2) study the system behavior with relativistic beams; and 3) study angular-dependent modes of interaction.

The experimental work will be largely concerned with the injection of a beam into the plasma outside the core of the hollow cathode arc. Both beam-plasma electron and beam-plasma ion interactions will be studied. If time permits, we will undertake the study of systems in which the beam is reflected back along the axis.

Electron-Cyclotron Heating of a Plasma. A system has been built for heating a plasma in a TE_{010} cavity. The gas will be pre-ionized by a low-power (50 watt) 10 cm, cw source. A 10 μsec, 10 cm, high power (1/2-1 Mw) pulse will be used to heat the plasma.

Theory of Active and Passive Anisotropic Plasma Waveguides. Guided waves are being studied for which the quasistatic approximation is not valid. A general theory of active and passive anisotropic plasma and electron beam waveguides is being developed. Theory of the interaction between a relativistic electron beam and a plasma will be studied.

Magnetohydrodynamic Power Generation. The theoretical work on ac power generation through magnetohydrodynamic interaction of a circuit with waves in a moving fluid will be continued. Large signal solutions will be evaluated for the one-dimensional case using a computer. Simultaneously, we shall search for simple analytic, large signal, solutions, which should serve as a guide towards an understanding

*This work was supported in part by the National Science Foundation under Grant G-9330; and in part by the U.S. Navy (Office of Naval Research) under Contract Nonr-1841(78).

of the computer solutions.

The small signal solutions obtained thus far will be studied in further detail both for the Alfvén wave amplifier and the compressional wave amplifier to find all existing modes.

L. D. Smullin, H. A. Haus, A. Bers

2. Highly Ionized Plasma and Fusion Research

This group is concerned principally with the study of highly ionized plasmas and their possible application to nuclear energy conversion.

Plasma Kinetic Theory. Calculation of the generation and transport of radiation (for example, cyclotron radiation) in a plasma and of other plasma properties derivable from plasma correlation will continue.

Plasma Diffusion. Theoretical and experimental determination of the diffusion of a highly ionized plasma cylinder of finite length, with and without conducting boundaries, will be completed during the coming year, by using the very successful hollow-cathode plasma source.

Plasma Acceleration. We are making studies on the acceleration of a highly ionized plasma to a velocity of approximately 10^5 m/sec, using a 2m plasma column and pulsed traveling-wave line.

Field Systems for Nonadiabatic Particle Motion. The synchronous injection scheme ("Corkscrew") for long-time trapping of charged particles in magnetic-field structures has proved to be very interesting. Theoretical and experimental studies (by using electrons) continue on the possibility of achieving very long time trapping in magnetic mirrors and in other structures.

Superconducting Magnets. A large superconducting solenoid with room temperature working space of approximately 0.05 m^3 is being constructed to operate at 2.5 webers/m^2. Basic problems of mechanical support, magnetic and mechanical stress, and so forth are being solved. Such solenoids will be vital for large plasma confinement.

Thermonuclear Blanket Studies. Calculations are under way on the conceptual design of energy-extraction blankets for fusion reactors, including neutron slowing down, multiplication, and capture; and on tritium regeneration and heat transfer. Experimental study of a mock-up assembly has begun.

Ion Beams. Experiments have started on the production of high-current and low-divergence ion beams, neutralized at least in part by properly designed electron space charge.

Cesium Plasmas. With a view to eventual electrical energy conversion from nuclear heat and other prime sources, the physical properties of the cesium plasma itself and a number of experimental devices are being studied.

Controlled-Fusion Plasma. It appears possible to design a large fusion plasma experiment with hope of success, by using a number of the developments listed above. Preliminary calculations for such a system will be made.

D. J. Rose

A. EXTENSION OF A BIDIRECTIONAL WAVEGUIDE THEOREM

In his study of "bidirectional" waveguides, Chorney[1] has derived and discussed, for one wave (either propagating, cutoff, or complex) with propagation constant

$\gamma = \alpha + j\beta$, the formulas

$$\alpha(P+jQ) = j\omega(U_m - U_e) \tag{1}$$

$$\beta(P+jQ) = \omega(U_T - U_z) \tag{2}$$

where $P + jQ$ is the complex power flowing down the waveguide, and U_m, U_e, U_T, and U_z are, respectively, the magnetic, electric, transverse, and longitudinal "pseudo energies" per unit length of the guide.[1]

We derive here the extensions of Eqs. 1 and 2 for waveguides that need not be bidirectional. Then we extend these formulas to electron-beam and plasma waveguides, following a previous study[2] of conservation principles in electron beams and plasmas.

We assume first that the waveguide may be partially or completely filled with a material that is linear and lossless, and may be anisotropic, nonreciprocal, and dispersive, but uniform in the z-direction. It is described by $\bar{\bar{\epsilon}}$ and $\bar{\bar{\mu}}$ tensors that are functions of the transverse coordinates x and y, and of frequency $j\omega$ (more generally, of complex frequency $s = \sigma + j\omega$). The waveguide is enclosed by a material that is, at every point, either a perfect electric conductor (with no tangential $\bar{E}$-field) or a perfect magnetic conductor (with no tangential $\bar{H}$-field). We start with Maxwell's equations for exponentially time-variant fields without free current:

$$\nabla \times \bar{H} = s\bar{D} \tag{3}$$

$$\nabla \times \bar{E} = -s\bar{B}. \tag{4}$$

These equations split into transverse components (with subscript T) and longitudinal components (with subscript z):

$$-\frac{\partial \bar{E}_T}{\partial z} = -s\bar{i}_z \times \bar{B}_T - \nabla_T E_z \tag{5}$$

$$0 = \bar{i}_z \cdot \nabla_T \times \bar{H}_T - sD_z \tag{6}$$

$$-\frac{\partial \bar{H}_T}{\partial z} = s\bar{i}_z \times \bar{D}_T - \nabla_T H_z \tag{7}$$

$$0 = \bar{i}_z \cdot \nabla_T \times \bar{E}_T + sB_z. \tag{8}$$

Since the excitation is assumed to be a wave, all field quantities have the z-dependence, $e^{-\gamma z}$, where γ is the complex propagation constant $\gamma = \alpha + j\beta$. Thus $\partial/\partial z$ is equivalent to multiplication by $-\gamma$, so Eqs. 5 and 7 are equal, respectively, to $\gamma\bar{E}_T$ and $\gamma\bar{H}_T$.

For the case of immediate interest, the excitation is sinusoidal, so that $s = j\omega$. Let us dot-multiply Eq. 5 by $\left(\bar{H}_T^* \times \bar{i}_z\right)$, and add the complex conjugate of Eq. 6 multiplied by E_z.

In a similar way, we operate on Eqs. 7 and 8.

If we integrate the results over the cross-section area of the waveguide, we find two equations, the sum and difference of which are

$$\alpha(P+jQ) = j\omega(U_1+U_2-U_3-U_4) \tag{9}$$

$$\beta(P+jQ) = \omega(U_1-U_2+U_3-U_4) \tag{10}$$

where the complex power down the waveguide is

$$P + jQ = \frac{1}{2}\int_A \bar{\bar{E}} \times \bar{\bar{H}}^* \cdot \bar{i}_z \, da$$

$$= \frac{1}{2}\int_A \bar{\bar{E}}_T \times \bar{\bar{H}}_T^* \cdot \bar{i}_z \, da, \tag{11}$$

and the four "pseudo energies" U_1, U_2, U_3, and U_4, are:

$$U_1 = \frac{1}{4}\int_A \bar{\bar{H}}_T^* \cdot \bar{B}_T \, da \tag{12}$$

$$U_2 = \frac{1}{4}\int_A H_z^* B_z \, da \tag{13}$$

$$U_3 = \frac{1}{4}\int_A \bar{\bar{E}}_T \cdot \bar{\bar{D}}_T^* \, da \tag{14}$$

$$U_4 = \frac{1}{4}\int_A E_z D_z^* \, da. \tag{15}$$

(Note that these "pseudo energies" are complex numbers, not necessarily real.)

Equation 9 is exactly Eq. 1, so that the extension of Eq. 1 to nonbidirectional waveguides is of the same form. Also, whenever the tensors $\bar{\bar{\mu}}$ and $\bar{\bar{\epsilon}}$ have zero elements in the z-row and column, except for μ_{zz} and ϵ_{zz}, so that the waveguide is bidirectional,[1] U_1, U_2, U_3, and U_4 are real, and $U_1 + U_3$ is what Chorney calls the "transverse pseudo energy" U_T, and $U_2 + U_4$ is what Chorney calls the "longitudinal pseudo energy" U_z. Then, Eq. 10 reduces to Eq. 2. On the other hand, if the waveguide is not bidirectional, Eq. 10 is the logical extension of Eq. 2.

In general, for nonbidirectional waveguides, the right-hand side of Eq. 10 is not real, so that for waves with $\beta \neq 0$, the reactive power need not vanish. Perhaps the study of nonbidirectional waveguides, such as those containing ferrites or plasmas with arbitrary direction of steady magnetic field, can be simplified by interpreting the "pseudo energy" terms in Eq. 10.

The preceeding discussion applies to plasma waveguides only if one is willing to "suppress" knowledge of the mechanical variables by using a tensor $\bar{\bar{\epsilon}}$ to describe the plasma. On the other hand, insight is obtained by considering explicitly the mechanical variables.

The extension of Eqs. 1 and 2 to a waveguide system containing an electron beam or a plasma is based on a previous study of conservation theorems for such systems.[2] Thus, for electron-beam systems[3] for which

$$\bar{J}_T^* \cdot \left[\bar{v}\times(\nabla\times\bar{p})\right]_T = 0 \tag{16}$$

and

$$J_z\left[\bar{v}\times(\nabla\times\bar{p})\right]_z = 0 \tag{17}$$

we find

$$\alpha(P+jQ) = j\omega(U_1+U_2-U_3-U_4+U_5+U_6) \tag{18}$$

$$\beta(P+jQ) = \omega(U_1-U_2+U_3-U_4-U_5+U_6+U_7), \tag{19}$$

where U_1, U_2, U_3, and U_4 are given by Eqs. 12-15 with the simpler constitutive relations, $\bar{B} = \mu_o\bar{H}$ and $\bar{D} = \epsilon_o\bar{E}$, and

$$U_5 = \frac{1}{4}\int_A \frac{\rho_o}{q}\,\bar{v}_T^* \cdot (m\bar{v})_T\,da \tag{20}$$

$$U_6 = \frac{1}{4}\int_A \frac{\rho_o}{q}\,v_z^*(mv)_z\,da \tag{21}$$

$$U_7 = \frac{1}{2}\int_A v_{oz}\,\frac{(mv)_z\,\rho^*}{q}\,da. \tag{22}$$

The remaining symbols have been defined[2]. Note particularly that the complex power P + jQ now has both an electromagnetic and a kinetic part:

$$P + jQ = \frac{1}{2}\int_A \left[\bar{E}\times\bar{H}^* + \frac{T}{q}\bar{J}^*\right] \cdot \bar{i}_z\,da. \tag{23}$$

Note from Eq. 18 that $\alpha P = 0$. On the other hand, even though U_1, U_2, U_3, and U_4 are now real, in general U_5, U_6, and U_7 are complex, so that βQ need not vanish. The "kinetic pseudo energies" U_5 and U_6 are complex (although their sum is real) for relativistic flow, if the unperturbed velocity $\bar{v}_o$ is neither parallel nor perpendicular to the z-direction. The quantity U_7 can be complex even for nonrelativistic flow, when the electrons have both an unperturbed and a perturbed velocity in the z-direction.

A convenient form of Eq. 19 is

$$\beta(P+jQ) = \omega(U_1+U_3-U_2-U_4-U_5-U_6+U_8), \tag{24}$$

where

$$U_8 = \frac{1}{2}\int_A (mv)_z \frac{J_z^*}{q}\, da \tag{25}$$

is related to the z-component of the complex kinetic power flow. In the right-hand side of Eq. 24, only the term U_8 is complex.

On the other hand, for plasmas, with $\bar{v}_o = 0$, the resulting extensions of Eqs. 1 and 2 turn out to be

$$\alpha(P+jQ) = j\omega[U_1+U_2-U_3-U_4+U_5+U_6-U_9] \tag{26}$$

$$\beta(P+jQ) = \omega[U_1+U_3-U_2-U_4-U_5+U_6+U_{10}] + j\omega U_{11} \tag{27}$$

where U_9, U_{10}, U_{11} are the real quantities

$$U_9 = \frac{1}{2}\int_A \rho_o \frac{\bar{v}_r \times \bar{v}_i}{\omega} \cdot \mu_o \bar{H}_o\, da \tag{28}$$

$$U_{10} = \frac{1}{2}\int_A \rho_o \frac{\bar{v}_{Tr} \times \bar{v}_{Ti}}{\omega} \cdot \bar{i}_z \mu_o H_{oz}\, da \tag{29}$$

$$U_{11} = \frac{1}{4}\int_A \rho_o \frac{\bar{i}_z \times \left(\bar{v}_T v_z^* + \bar{v}_T^* v_z\right)}{\omega} \cdot \mu_o \bar{H}_{oT}\, da. \tag{30}$$

For a traveling wave, the reactive power must vanish only when there is no dc magnetic field transverse to the waveguide.

For bidirectional waveguides, Eq. 2 is expressed in terms of the "transverse" and the "longitudinal" pseudo energies. When the mechanical motion of the charges is considered explicitly, such nomenclature, even for the very simplest cases, is inappropriate because the kinetic terms come into Eqs. 19 and 27 with the wrong sign. The transverse kinetic terms add with the longitudinal electromagnetic terms, and vice versa.

Note from Eqs. 18 and 26 that if any net real power P is carried by a single wave, then that wave can neither grow nor decay, since $\alpha = 0$. Therefore, for growing waves, either cutoff ($\beta=0$) or complex ($\beta\neq0$), we find $P = 0$. These waves carry no net power. However, such waves in an electron beam (not a plasma, which has $T = 0$) can carry

net electromagnetic power, provided that it is exactly balanced by a negative kinetic power. Such growing waves have the "pseudo-resonance" condition that the real parts of the right-hand sides of Eqs. 19 and 24 vanish.

P. Penfield, Jr., A. Bers

References

1. P. Chorney, Power and Energy Relations in Bidirectional Waveguides, Sc.D. Thesis, Department of Electrical Engineering, M.I T., September 1961.

2. A. Bers and P. Penfield, Jr., Conservation principles for plasmas and relativistic electron beams (submitted to Trans. IRE, PGED).

3. Ibid.; Note that these restrictions are different from those preceeding Eqs. (32), (39), (44), and (79) loc. cit.

B. A NEW DERIVATION OF SOME WAVEGUIDE THEOREMS

We present a new derivation of two waveguide theorems[1] relating phase velocity, group velocity, and the stored energy density of a single wave propagating in a waveguide. The waveguide may contain material that is linear, time-invariant, and lossless, and may, in general, be anisotropic, nonreciprocal, dispersive, and inhomogeneous, but the waveguide and material must be uniform in the propagation (z) direction.

The derivation is based upon the fact that for a dependence $\exp(st-\Gamma z)$, the material constants $\bar{\bar{\epsilon}}$ and $\bar{\bar{\mu}}$, the field amplitudes $\bar{E}$ and $\bar{H}$, and the propagation constant Γ, all of which are, in general, complex, are functions of the complex variable $s = \sigma + j\omega$. Except in special circumstances (for example, at a resonance or cutoff) when analyticity fails, the real and imaginary parts of these quantities must be related by the Cauchy-Riemann equations. It is this last property that we exploit in the derivations.

We begin with the relations that logically precede Eqs. 9 and 10 of Penfield and Bers (see Sec. XV-A), in which the s-dependence has been retained.

$$(\alpha+j\beta)(P+jQ) = 2sU_1 + 2s^*U_4 \tag{1}$$

$$(\alpha-j\beta)(P+jQ) = 2sU_2 + 2s^*U_3. \tag{2}$$

U_1, U_2, U_3, U_4, P, and Q have been defined by Penfield and Bers.

Let $s = \sigma + j\omega$ and write each of the pseudo-energy densities in terms of its real and imaginary parts ($U_1=U_{1R}+jU_{1I}$). Equating real and imaginary parts of Eqs. 1 and 2, and then adding and subtracting, we have

$$\alpha P = \sigma(U_{mR}+U_{eR}) - \omega(U_{mI}-U_{eI}) \tag{3}$$

$$\beta Q = \sigma(U_{2R}+U_{3R}-U_{1R}-U_{4R}) - \omega(U_{2I}-U_{3I}-U_{1I}+U_{4I}) \tag{4}$$

$$\alpha Q = \sigma(U_{mI}+U_{eI}) + \omega(U_{mR}-U_{eR}) \tag{5}$$

$$\beta P = \sigma(U_{1I}+U_{4I}-U_{2I}-U_{3I}) + \omega(U_{1R}+U_{3R}-U_{2R}-U_{4R}) \tag{6}$$

We have used the symbols U_m and U_e for the total magnetic and electric pseudo-energy densities per unit length.

$$U_m = U_1 + U_2 = \frac{1}{4}\iint_A (\bar{H}^* \cdot \bar{\bar{\mu}} \cdot \bar{H})\, dA \tag{7}$$

$$U_e = U_3 + U_4 = \frac{1}{4}\iint_A (\bar{E} \cdot \bar{\bar{\epsilon}}^* \cdot \bar{E}^*)\, dA \tag{8}$$

Differentiate Eq. 3 with respect to σ, and then set $\sigma = 0$ and $\alpha = 0$ because we are interested in a purely propagating (undamped) wave.

$$P\frac{\partial \alpha}{\partial \sigma} = (U_{mR}+U_{eR}) - \omega\frac{\partial}{\partial \sigma}(U_{mI}-U_{eI}) \tag{9}$$

Immediately $\partial\alpha/\partial\sigma$ can be replaced by $\partial\beta/\partial\omega$ (Cauchy-Riemann), but the evaluation of the σ-derivative of the pseudo-energy densities is not quite as straightforward. Because U_m and U_e contain the complex conjugate of a field quantity, neither is a function of the complex variable s, although the field amplitudes and $\bar{\bar{\epsilon}}$ and $\bar{\bar{\mu}}$ of which U_m and U_e are composed are such functions.

Our task, then, is to convert the following σ-derivative into an ω-derivative.

$$\frac{\partial}{\partial \sigma}(U_{mI}-U_{eI}) = \frac{1}{4}\iint_A \frac{\partial}{\partial \sigma}\{\bar{H}^* \cdot \bar{\bar{\mu}} \cdot \bar{H} - \bar{E} \cdot \bar{\bar{\epsilon}}^* \cdot \bar{E}^*\}_I\, dA \tag{10}$$

Consider, for example, the term $\frac{\partial}{\partial \sigma}(\bar{H}^* \cdot \bar{\bar{\mu}} \cdot \bar{H})$. We first write $\bar{H} = \bar{H}_R + j\bar{H}_I$ and $\bar{\bar{\mu}} = \bar{\bar{\mu}}_R + j\bar{\bar{\mu}}_I$, and carry through the differentiation with respect to σ. Then using the Cauchy-Riemann equations to replace the σ-derivatives by ω-derivatives, we have

$$\frac{\partial}{\partial \sigma}(\bar{H}^* \cdot \bar{\bar{\mu}} \cdot \bar{H}) = j\frac{\partial \bar{H}^*}{\partial \omega} \cdot \bar{\bar{\mu}} \cdot \bar{H} - j\bar{H}^* \cdot \bar{\bar{\mu}} \cdot \frac{\partial \bar{H}}{\partial \omega} - j\bar{H}^* \cdot \frac{\partial \bar{\bar{\mu}}}{\partial \omega} \cdot \bar{H}. \tag{11}$$

Because the material is assumed to be lossless, $\bar{\bar{\epsilon}}$ and $\bar{\bar{\mu}}$ are Hermitian, so that the sum of the first two terms on the right-hand side of Eq. 11 is real. Then taking the imaginary part of Eq. 11, we have

$$\frac{\partial}{\partial \sigma}(\bar{H}^* \cdot \bar{\bar{\mu}} \cdot \bar{H})_I = -\left(\bar{H}^* \cdot \frac{\partial \bar{\bar{\mu}}}{\partial \omega} \cdot \bar{H}\right). \tag{12}$$

Similarly, we find that

$$\frac{\partial}{\partial\sigma}\left(\bar{E}\cdot\bar{\bar{\epsilon}}^{*}\cdot\bar{E}^{*}\right)_{I}=\left(\bar{E}^{*}\cdot\frac{\partial\bar{\bar{\epsilon}}}{\partial\omega}\cdot\bar{E}\right). \tag{13}$$

Thus

$$\frac{\partial}{\partial\sigma}\left(U_{mI}-U_{eI}\right)=-\frac{1}{4}\iint_{A}\left\{\bar{H}^{*}\cdot\frac{\partial\bar{\bar{\mu}}}{\partial\omega}\cdot\bar{H}+\bar{E}^{*}\cdot\frac{\partial\bar{\bar{\epsilon}}}{\partial\omega}\cdot\bar{E}\right\}dA. \tag{14}$$

Now, because $\bar{\bar{\epsilon}}$ and $\bar{\bar{\mu}}$ are Hermitian,

$$U_{mR}+U_{eR}=\frac{1}{4}\iint_{A}\left\{\bar{H}^{*}\cdot\bar{\bar{\mu}}\cdot\bar{H}+\bar{E}^{*}\cdot\bar{\bar{\epsilon}}\cdot\bar{E}\right\}dA \tag{15}$$

so that

$$\left(U_{mR}+U_{eR}\right)-\omega\frac{\partial}{\partial\sigma}\left(U_{mI}-U_{eI}\right)=\frac{1}{4}\iint_{A}\left\{\bar{H}^{*}\cdot\frac{\partial(\omega\bar{\bar{\mu}})}{\partial\omega}\cdot\bar{H}+\bar{E}^{*}\cdot\frac{\partial(\omega\bar{\bar{\epsilon}})}{\partial\omega}\cdot\bar{E}\right\}dA. \tag{16}$$

We recognize the right-hand side of Eq. 16 as being W, the total time-average energy stored per unit length.

$$W=\left(U_{mR}+U_{eR}\right)-\omega\frac{\partial}{\partial\sigma}\left(U_{mI}-U_{eI}\right). \tag{17}$$

Putting this result into Eq. 9, we have

$$\frac{\partial\beta}{\partial\omega}=\frac{W}{P}. \tag{18}$$

This is the well-known result that the group velocity, $v_g=\left(\frac{\partial\beta}{\partial\omega}\right)^{-1}$, is equal to the energy velocity, that is, the power per unit area divided by the true energy stored per unit length.

Setting $\sigma = 0$ in Eq. 6, we find that

$$\frac{\beta}{\omega}=\frac{U_{1R}+U_{3R}-U_{2R}-U_{4R}}{P} \tag{19}$$

The combination of Eqs. 18 and 19 gives

$$\frac{\partial\beta}{\partial\omega}=\frac{\beta}{\omega}\frac{W}{U_{1R}+U_{3R}-U_{2R}-U_{4R}}. \tag{20}$$

When $\bar{\bar{\epsilon}}$ and $\bar{\bar{\mu}}$ have zero elements in the z-row and column, except for ϵ_{zz}, and μ_{zz}, so that the waveguide is bidirectional,[1] U_1, U_2, U_3, and U_4 are real, and we can drop the subscript R in Eqs. 19 and 20. Then (U_1+U_3) is Chorney's "transverse pseudo energy

per unit length," U_T, and (U_2+U_4) is the "longitudinal pseudo energy per unit length," U_z.

$$\frac{\partial\beta}{\partial\omega} = \frac{\beta}{\omega}\frac{W}{U_T - U_z} \tag{21}$$

For the bidirectional waveguide we can proceed in a similar manner and obtain an analogous result for a cutoff wave. We differentiate Eq. 4 with respect to σ and then set $\sigma = 0$ and $\beta = 0$. The Cauchy-Riemann equations then yield

$$\frac{\partial\alpha}{\partial\omega} = \frac{(W_{mT}-W_{mz}) - (W_{eT}-W_{ez})}{Q}. \tag{22}$$

Setting $\sigma = 0$ in Eq. 5, we have

$$\frac{\alpha}{\omega} = \frac{U_m - U_e}{Q}. \tag{23}$$

Elimination of Q between the last two equations gives the analogue of Eq. 21.

$$\frac{\partial\alpha}{\partial\omega} = \frac{\alpha}{\omega}\frac{(W_{mT}-W_{mz}) - (W_{eT}-W_{ez})}{U_m - U_e}. \tag{24}$$

Although the expressions derived here are not new, their derivation, based upon the Cauchy-Riemann equations, appears to be novel. The extension to electron beams and plasmas is being studied.

A. J. Schneider

References

1. P. Chorney, Power, energy, group velocity, and phase velocity in bidirectional waveguides, Quarterly Progress Report No. 60, Research Laboratory of Electronics, M. I. T., January 15, 1961, pp. 37-46.

C. A LARGE-SIGNAL, STEADY-STATE SOLUTION FOR A ONE-DIMENSIONAL PLASMA COUPLED TO A TRAVELING-WAVE CIRCUIT

Theoretical information about the efficiency and saturation power of magnetohydrodynamic ac generators[1] is possible only through a large-signal analysis of the circuit-fluid interaction. Detailed large-signal analyses will be made on a computer. However, the understanding of the computer results will be increased if we are able to find a number of simple closed-form large-signal solutions. The solution reported on here was derived with such a purpose in mind.

We have found an interesting large-signal, self-consistent, steady-state solution in which rectangular wave-shaped profiles of density, pressure, and magnetic field are "frozen" into the plasma which travels with a uniform velocity v_o. The profile is held

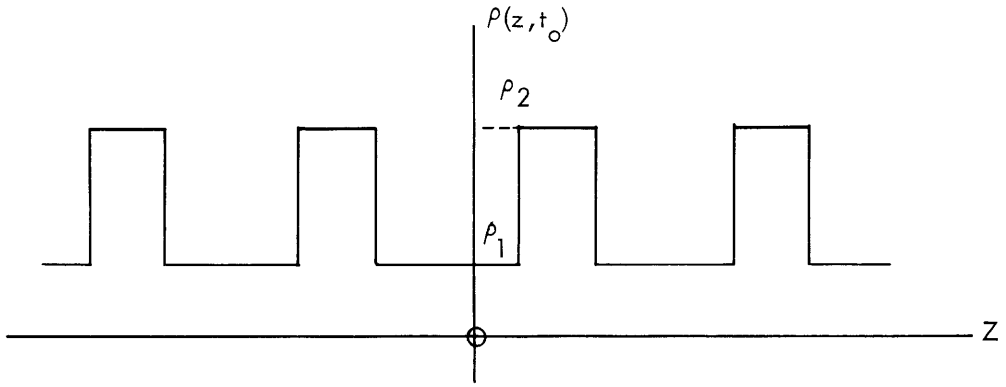

Fig. XV-1. Density distribution as a function of distance.

in equilibrium by current sheets located at the planes of discontinuity, the current sheets being produced by rectangular pulses of voltage and current which travel along the circuit in synchronism with the plasma. Figure XV-1 shows the profile of density as a function of distance z in the direction of motion. The pressure and magnetic field have similar distributions.

Equations 1-9 are the large-signal equations that we use.

Plasma

$$\rho\left(\frac{\partial v}{\partial t} + v\frac{\partial v}{\partial z}\right) = -\frac{\partial p}{\partial z} - JB \tag{1}$$

$$\frac{\partial \rho}{\partial t} + \frac{\partial}{\partial z}(v\rho) = 0 \tag{2}$$

$$\frac{1}{\mu_o}\frac{\partial B}{\partial z} = J + J_D \tag{3}$$

$$\frac{\partial E}{\partial z} = \frac{\partial B}{\partial t} \tag{4}$$

$$E = -vB \tag{5}$$

$$p = \frac{p_o}{\rho_o^\gamma}\rho^\gamma \tag{6}$$

Circuit

$$\frac{\partial V}{\partial z} = -L\frac{\partial I}{\partial t} + nw\frac{\partial B}{\partial t} \tag{7}$$

$$\frac{\partial I}{\partial z} = -C\frac{\partial V}{\partial t} \tag{8}$$

$$J_D = -\frac{n}{h}\frac{\partial I}{\partial z} \tag{9}$$

Every fluid particle moves with the constant velocity v_o, so that Eq. 1 reduces to

$$\frac{\partial p}{\partial z} = -JB. \tag{10}$$

Equilibrium demands that there be sheets of plasma current located at the planes of discontinuity. These current sheets interact with the magnetic field according to Eq. 10 to produce forces that balance the expansive pressure forces caused by the density gradient. On the other hand, the discontinuities in the magnetic field call for current sheets of $J + J_D$ (plasma current plus driving current from the circuit) which satisfy Eq. 3. It is easily shown that J_D and J must be oppositely directed and that the magnitude of J_D exceeds that of J.

We proceed analytically by assuming a solution of the form indicated in Fig. XV-1 for the density, pressure, and magnetic field. When we substitute this solution formally into Eqs. 2-10 we arrive at a relationship between the plasma velocity v_o, ρ_1 and ρ_2, the values of density on either side of the discontinuity.

$$\left(\frac{\rho_2 + \rho_1}{2}\right)\left(\frac{\rho_2 - \rho_1}{\mu_o}\right)\left[\frac{n^2\mu_o C w v_o^2}{h(1-v_o^2LC)} - 1\right] = \frac{p_o}{B_o^2\rho_o^{\gamma-2}}\left(\rho_2^\gamma - \rho_1^\gamma\right) \tag{11}$$

We imagine the profile to have been created sometime in the remote past from an initially uniform plasma characterized by the parameters ρ_o, p_o, B_o and v_o. Therefore, no material crosses the planes of discontinuity; the initial bunching (the choice of pulse width and pulse separation), together with Eq. 11, determines all of the variables.

The bracketed term in Eq. 11 must be positive. Zero coupling (n=0) implies the solution $\rho_1 = \rho_2$, so that the discontinuities cannot exist in the plasma in the absence of the guidance provided by the circuit. Also evident is the fact that v_o must be less than $v_p = (LC)^{-1/2}$, the phase velocity of a wave traveling along the circuit in the absence of the plasma. At constant amplitude, decreasing the coupling between circuit and plasma increases synchronism between v_o and v_p — exactly what would be expected physically. It should be borne in mind, however, that v_p is the phase velocity of the circuit wave only for weak coupling.

The special case $\gamma = 2$, corresponding to two internal degrees of freedom is interesting because Eq. 11 for v_o becomes independent of the jump in density. This is a much less stringent condition for the existence of a solution than Eq. 11 with $\gamma \neq 2$.

Thus far, we have done nothing more than verify the fact that the rectangular profile does indeed satisfy the equations. The solution appears to be stable but this conjecture has yet to be verified quantitatively.

H. A. Haus, A. J. Schneider

References

1. H. A. Haus, Magnetohydrodynamic ac generator, Quarterly Progress Report No. 60, Research Laboratory of Electronics, M.I.T., January 15, 1961, pp. 46-50.

D. ELECTRON BEAM-PLASMA INTERACTION EXPERIMENTS*

An apparatus has been built for the study of the interaction of an electron beam with a steady-state plasma. The source of plasma is a hollow-cathode discharge similar to the one previously described by Getty and Smullin.[1,2] A cathode of 1/8 in. O.D. tantalum tubing, through which argon is passed, allows the arc to run steadily for many hours. The chamber containing the plasma is evacuated by two 4-inch oil-diffusion pumps that have a combined pumping speed of approximately 1400 liters per second, thereby permitting the arc to run in a stable manner at pressures of less than 1×10^{-4} mm Hg. At pressures of 2 or 3×10^{-4} mm Hg, the arc will run at a minimum current of approximately 3 amps, and at a maximum current of greater than 100 amps. Densities in the center of the arc may be in the range 10^{11}-10^{13} electrons per cubic centimeter with approximately 30 per cent of the gas ionized. At a distance of approximately 1 inch from the center of the arc, probe measurements indicate the plasma density has fallen to approximately 10 per cent of its maximum value.

The electron gun used in these experiments will produce a current of 1 amp at an accelerating voltage of 10 kv. It is mounted in a chamber that is connected to the main plasma chamber by the small hole through which the beam passes. When the system is in operation, the pressure in the gun chamber (approximately 5×10^{-6} mm Hg) is

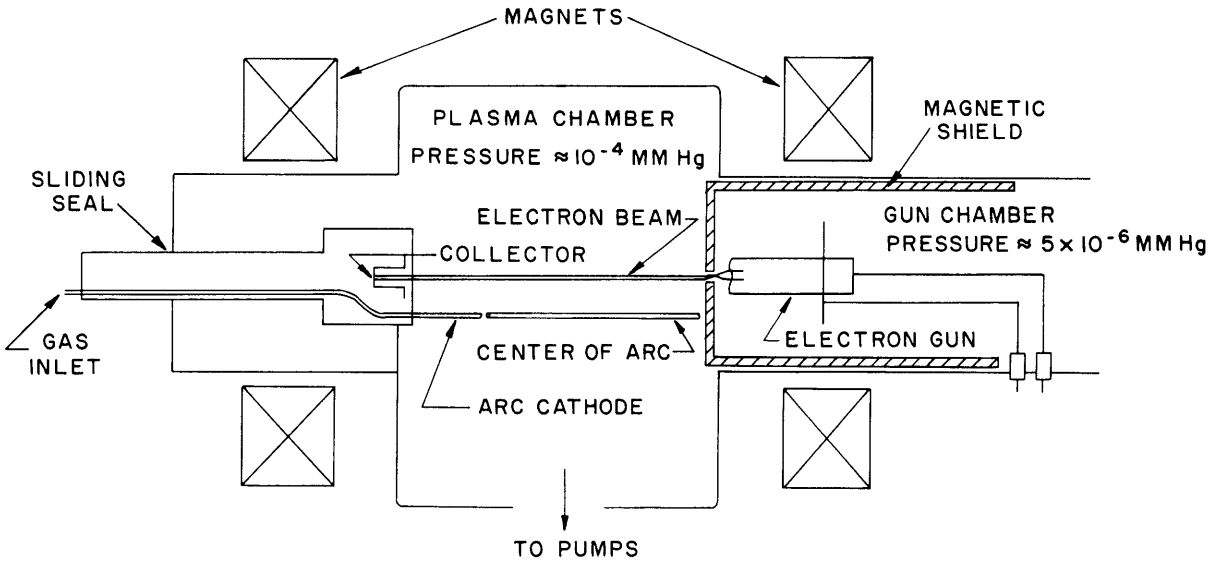

Fig. XV-2. Main components of beam-plasma interaction apparatus.

*This research was supported in part by Purchase Order DDL B-00306 with Lincoln Laboratory, a center for research operated by Massachusetts Institute of Technology with the joint support of the U.S. Army, Navy, and Air Force under Air Force Contract AF19(604)-7400.

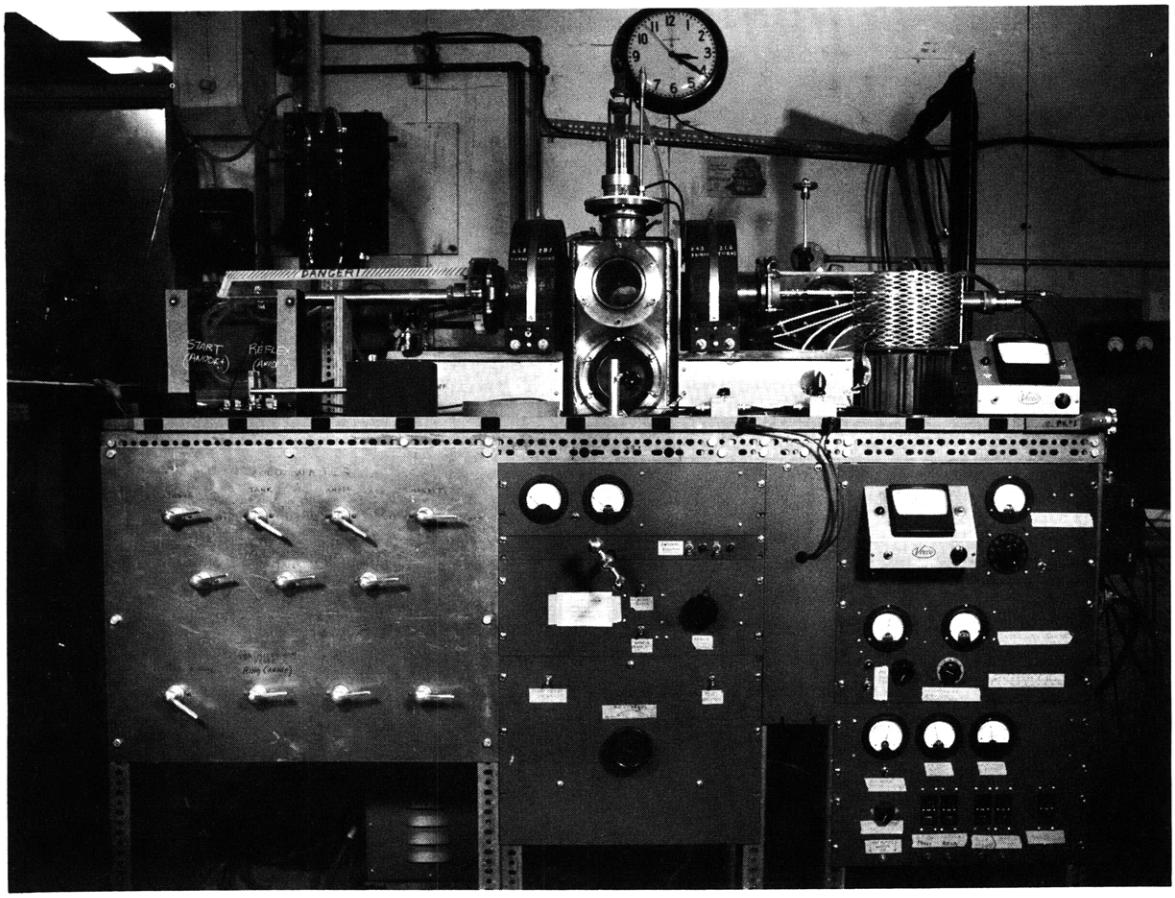

Fig. XV-3. Beam-plasma interaction experimental apparatus.

maintained by a separate oil-diffusion pump.

Two magnets are used to supply a magnetic field in the range 0-1000 gauss which is coaxial with the beam. The electron gun is mounted on the magnetic axis of the system, while the arc is run approximately 1 inch away from the axis to prevent damage to the gun. Figure XV-2 shows the general orientation of the main components of the system.

Only preliminary experiments have been conducted to determine whether or not all components of the system are working properly. A detailed investigation of the spectra of the rf power and visible light radiated from the system is being proposed. A photograph of the apparatus appears as Fig. XV-3.

D. L. Morse

References

1. W. D. Getty, A low-pressure gas arc device, Quarterly Progress Report No. 57, Research Laboratory of Electronics, M.I.T., April 15, 1960, pp. 27-29.

2. W. D. Getty and L. D. Smullin, Experimental results of the study of the hollow-cathode discharge, Quarterly Progress Report No. 58, Research Laboratory of Electronics, M.I.T., July 15, 1960, pp. 35-41.

E. INTERACTION BETWEEN AN ELECTRON BEAM AND PLASMA*

In our previous report[1] we derived the dispersion equation for the interaction between an electron beam and plasma. In this report we examine the fields associated with this interaction.

1. Model and Procedure

Our model for the plasma is one with ions of negligible thermal velocities and electrons with a thermal spread of velocities without a superimposed drift velocity. The electrons have a uniform density and are neutralized by ions of finite mass. The electrons in the beam have a well-defined velocity along the axis of the waveguide.

The waveguide is a hollow, uniform, metal tube of arbitrary cross section. Therefore we shall use a system of generalized orthogonal coordinates u_1, u_2, z, with the z-axis taken parallel to the axis of the waveguide. There is a uniform, finite, axial, magnetostatic field along the axis of the waveguide.

Our treatment is non-quasistatic and makes use of the small-signal theory. We use a matrix formulation of the equations. We neglect nonuniformities and pressure gradients. At first, we neglect the temperature of the plasma electrons as well as collisions. Then we examine the modifications of the derived equations by temperature effects. We neglect relativistic effects. The ac quantities vary harmonically with time and we shall omit the factor $\exp(j\omega t)$.

First we derive the dielectric tensor and the $[\zeta]$ tensor defining a Tellegen medium.[2] This is because of the initial velocity of the beam, which converts our system from a gyroelectric medium to a Tellegen medium. Then we solve Maxwell's equations for the electric and magnetic fields. The final equations are coupled because of the magnetic field, and are of the same type as Van Trier's equations,[3] but with modified coefficients because of the initial velocity of the beam. We also derive the dispersion equation, which coincides with our previous one,[1] and the boundary conditions. Finally, we specialize our results for useful geometries.

2. Dielectric Tensor

From Lorentz's force equation,

$$m_m \frac{d\bar{v}_m}{dt} = e_m(\bar{E} + \bar{v} \times \bar{B}), \tag{1}$$

*This research was supported in part by Purchase Order DDL B-00306 with Lincoln Laboratory, a center for research operated by Massachusetts Institute of Technology with the joint support of the U.S. Army, Navy, and Air Force under Air Force Contract AF19(604)-7400.

we find that

$$[v_m] = j\eta_m[M_m][E], \tag{2a}$$

where

$$[M_m] = \begin{bmatrix} \dfrac{\omega - \beta_z v_{om}}{\omega_{cm}^2 - (\omega-\beta_z v_{om})^2} & -j\dfrac{\omega_{cm}}{\omega_{cm}^2 - (\omega-\beta_z v_{om})^2} & 0 \\ \dfrac{j\omega_{cm}}{\omega_{cm}^2 - (\omega-\beta_z v_{om})^2} & \dfrac{\omega - \beta_z v_{om}}{\omega_{cm}^2 - (\omega-\beta_z v_{om})^2} & 0 \\ 0 & 0 & -\dfrac{1}{\omega - \beta_z v_{om}} \end{bmatrix} \tag{2b}$$

The parameter m can take on the values e for plasma electrons, i for plasma ions, and b for beam electrons, $\omega_{cm} = \eta_m B_o$.

The ac charge density is given by

$$\rho_m = j\rho_{om}\frac{\nabla \cdot \bar{v}_m}{\omega - v_{om}\beta_z} \tag{3}$$

and the ac current density is given by

$$\bar{J}_m = \rho_{om}\bar{v}_m + \rho_m\bar{v}_{om}. \tag{4a}$$

If we write $\bar{v}_m$ and ρ_m as functions of $\bar{E}$ by use of Eqs. 2 and 3, we find for the total current density $\left(\bar{J} = \sum_m \bar{J}_m\right)$ that:

$$[J] = j\omega\left([\epsilon]' - \epsilon_o[I]\right)[E], \tag{4b}$$

where

$$[\epsilon]' = \left[\begin{array}{c|c|c} \epsilon_1 & -j\epsilon_2 & 0 \\ \hline j\epsilon_2 & \epsilon_1 & 0 \\ \hline j\dfrac{\epsilon_4}{\beta_z}\dfrac{1}{h_1h_2}\dfrac{\partial}{\partial u_1}(h_2 & \dfrac{\epsilon_5}{\beta_z}\dfrac{1}{h_1h_2}\dfrac{\partial}{\partial u_1}(h_2 & \\ -\dfrac{\epsilon_5}{\beta_z}\dfrac{1}{h_1h_2}\dfrac{\partial}{\partial u_2}(h_1 & +j\dfrac{\epsilon_4}{\beta_z}\dfrac{1}{h_1h_2}\dfrac{\partial}{\partial u_2}(h_1 & \epsilon_3' \end{array}\right] \tag{5}$$

The values of the tensor elements are:

$$\epsilon_1 = \epsilon_o\left\{1 + \frac{1}{\omega}\sum_m \frac{\omega_{pm}^2(\omega-\beta_z v_{om})}{\omega_{cm}^2 - (\omega-\beta_z v_{om})^2}\right\} \tag{5a}$$

$$\epsilon_2 = \epsilon_o \frac{1}{\omega}\sum_m \frac{\omega_{pm}^2 \omega_{cm}}{\omega_{cm}^2 - (\omega-\beta_z v_{om})^2} \tag{5b}$$

$$\epsilon_3' = \epsilon_o\left\{1 - \sum_m \frac{\omega_{pm}^2}{(\omega-\beta_z v_{om})^2}\right\} \tag{5c}$$

$$\epsilon_4 = \epsilon_o \frac{\beta_z}{\omega}\sum_m \frac{v_{om}\omega_{pm}^2}{\omega_{cm}^2 - (\omega-v_{om}\beta_z)^2} \tag{5d}$$

$$\epsilon_5 = \epsilon_o \frac{\beta_z}{\omega}\sum_m \frac{v_{om}\omega_{pm}^2\omega_{cm}}{(\omega-v_{om}\beta_z)\left[\omega_{cm}^2-(\omega-v_{om}\beta_z)^2\right]}. \tag{5e}$$

Now, Maxwell's equations can be written

$$\nabla \times \overline{E} = -j\omega\mu_o \overline{H} \tag{6a}$$

$$\nabla \times \overline{H} = j\omega[\epsilon]' \overline{E}. \tag{6b}$$

To get rid of the derivatives inside the dielectric tensor, we write the z-component of Eq. 6b:

$$-\frac{1}{h_1h_2}\frac{\partial}{\partial u_2}(h_1H_1) + \frac{1}{h_1h_2}\frac{\partial}{\partial u_1}(h_2H_2) = j\omega\epsilon_3' E_z$$

$$-\frac{\omega\epsilon_4}{\beta_z}\left\{\frac{1}{h_1h_2}\frac{\partial}{\partial u_1}(h_2E_1) + \frac{1}{h_1h_2}\frac{\partial}{\partial u_2}(h_1E_2)\right\}$$

$$+j\frac{\omega\epsilon_5}{\beta_z}\left\{\frac{1}{h_1h_2}\frac{\partial}{\partial u_1}(h_2E_2) - \frac{1}{h_1h_2}\frac{\partial}{\partial u_2}(h_1E_1)\right\}. \tag{7}$$

By using the z-component of Eq. 6a and the conservation of charges, we find, after some algebraic manipulations, that

$$-\frac{1}{h_1h_2}\frac{\partial}{\partial u_2}(h_1H_1) + \frac{1}{h_1h_2}\frac{\partial}{\partial u_1}(h_2H_2) = j\omega\epsilon_3 E_z + \zeta_3 H_z, \tag{8a}$$

where $\epsilon_3 = \dfrac{\epsilon_3' \epsilon_1}{\epsilon_1 + \epsilon_4}$; that is

$$\epsilon_3 = \epsilon_o \left\{ 1 - \sum_m \frac{\omega_{pm}^2}{(\omega - \beta_z v_{om})^2} \right\} \left\{ 1 + \frac{1}{\omega} \sum_m \frac{\omega_{pm}^2 (\omega - \beta_z v_{om})}{\omega_{cm}^2 - (\omega - \beta_z v_{om})^2} \right\}$$

$$\times \left\{ 1 + \sum_m \frac{\omega_{pm}^2}{\omega_{cm}^2 - (\omega - \beta_z v_{om})^2} \right\}^{-1} \tag{8b}$$

and

$$\zeta_3 = \frac{\omega^2 \mu_o}{\beta_z} \left\{ \frac{\epsilon_5 \epsilon_1 - \epsilon_4 \epsilon_2}{\epsilon_1 + \epsilon_4} \right\}. \tag{8c}$$

Now, Eq. 6b can be rewritten as

$$\nabla \times \bar{H} = j\omega[\epsilon]\, \bar{E} + [\zeta]\, \bar{H}, \tag{9}$$

where

$$[\epsilon] = \begin{bmatrix} \epsilon_1 & -j\epsilon_2 & 0 \\ j\epsilon_2 & \epsilon_1 & 0 \\ 0 & 0 & \epsilon_3 \end{bmatrix}$$

and

$$[\zeta] = \begin{bmatrix} 0 & 0 & 0 \\ 0 & 0 & 0 \\ 0 & 0 & \zeta_3 \end{bmatrix}$$

The equations above show that our system has been converted from a gyroelectric medium to a Tellegen medium, because of the initial velocity of the beam ($\zeta_3 \to 0$ as $v_{om} \to 0$)

3. Solution of the Equations

From the transverse component equations (6a) and (9), we obtain

$$\bar{E}_t = \nabla_t (pE_z + rH_z) - \bar{i}_z \times \nabla_t (qE_z + sH_z) \tag{10a}$$

$$\bar{H}_t = \nabla_t (tE_z + pH_z) - \bar{i}_z \times \nabla_t (uE_z + qH_z) \tag{10b}$$

where p, q, r, s, t, u are the same functions of ϵ_1, ϵ_2, as in Van Trier's[3] treatment, but ϵ_1, ϵ_2, are now given by Eqs. 5a and 5b, and $\mu_1 = \mu_3 = \mu_o$, $\mu_2 = 0$; that is, the medium is not gyromagnetic.

For the longitudinal components we obtain from the longitudinal component equations (6a) and (9), by use of Eqs. 10,

$$\nabla_t^2 E_z + aE_z + bH_z = 0 \tag{11a}$$

$$\nabla_t^2 H_z + cH_z + dE_z = 0 \tag{11b}$$

where

$$a = \omega^2 \mu_o \epsilon_3 - \frac{\epsilon_3}{\epsilon_1} \beta_z^2 \tag{12a}$$

$$b = j\omega\mu_o \beta_z \frac{\epsilon_2 + \epsilon_5}{\epsilon_1 + \epsilon_4} \tag{12b}$$

$$c = \omega^2 \mu_o \frac{\epsilon_1^2 - \epsilon_2^2}{\epsilon_1 + \epsilon_4} - \beta_z^2 \tag{12c}$$

$$d = -j\omega \frac{\epsilon_3 \epsilon_2}{\epsilon_1} \beta_z . \tag{12d}$$

These coefficients are different from Van Trier's,[3] since they contain ϵ_4 and ϵ_5 (resulting from the $[\zeta]$ tensor); and also the rest of the elements of the dielectric tensor must be obtained from Eqs. 5a, 5b, and 8b.

The most general solutions of Eqs. 11 are:

$$E_z = E_{z1} + E_{z2} \tag{13a}$$

$$H_z = \frac{\beta_{t1}^2 - a}{b} E_{z1} + \frac{\beta_{t2}^2 - a}{b} E_{z2} \tag{13b}$$

where $\beta_{t1,2}$ are the solutions of

$$\beta_t^4 - (a+c)\beta_t^2 + ac - bd = 0. \tag{14}$$

Equations 11 and 13 give the complete solution of the field problem in the presence of an electron beam.

4. Dispersion Equation and Boundary Conditions

Equation 14 gives the transverse wave number as a function of the longitudinal wave number. We can obtain one more equation relating β_t and β_z by using the boundary conditions.

If we have a completely filled, metallic waveguide, then the boundary conditions are

$$E_z = E_2 = H_1 = 0. \tag{15}$$

These equations are not independent, as a consequence of Maxwell's equations.

If the waveguide is not completely filled by the plasma or the beam, we have to consider the equations

$$E_2, E_z, H_1, H_z = \text{continuous} \tag{16a}$$

$$E_1^{II} - E_1^{I} = \frac{j}{\epsilon_o} \sum_m \frac{\rho_{om}(v_{m1,II} - v_{m1,I})}{\omega - \beta_z v_{om}} \tag{16b}$$

$$H_2^{II} - H_2^{I} = j \sum_m \frac{\rho_{om} v_{om}(v_{m1,II} - v_{m1,I})}{\omega - \beta_z v_{om}} \tag{16c}$$

Here, we have assumed that the boundary is normal to u_1 and I and II refer to the regions inside and outside of the boundary surface (these equations are not independent). They have been derived by use of Hahn's method of replacing rippled ac surfaces by surface charges and currents.

Elimination of β_t between (14) (15), and (if necessary) (16), gives the dispersion equation of the propagation constant.

5. One-Dimensional Case

We find the following expressions for TEM waves (E_z=H_z=0):

$$\text{(i)}\quad \beta_z^3 - (\beta_e \pm \beta_{cb})\beta_z^2 - C\beta_z + C(\beta_e \pm \beta_{cb}) - k^2 \frac{\beta_{pb}^2}{\beta_e} = 0, \tag{17a}$$

where $\beta_{cb} = \omega_{ce}/v_{ob}$; $\beta_e = \omega/v_{ob}$; $\beta_{pb} = \omega_{pb}/v_{ob}$,

$$C = k^2 \left\{ 1 - \frac{\omega_{pe}^2}{\omega(\omega \pm \omega_{ce})} - \frac{\omega_{pi}^2}{\omega(\omega \pm \omega_{ci})} \right\}, \tag{17b}$$

and

$$E_1 = \pm jE_2 \tag{18a}$$

$$H_1 = \pm jH_2 = -\frac{\beta_z}{\omega\mu_o} E_2. \tag{18b}$$

This is the extension of Spitzer's EM waves when a beam interacts with a plasma.

(ii) For TM waves ($E_z \neq 0$),

$$\beta_z = \beta_e \pm \beta_p = \beta_e \pm \frac{\beta_{pb}}{\left(1 - \frac{\omega_{pi}^2 + \omega_{pe}^2}{\omega^2}\right)^{1/2}} \tag{19}$$

and

$$E_z = \left(E_{z+} e^{j\beta_p z} + E_{z-} e^{j\beta_p z}\right) e^{j(\omega t - \beta_e z)} \tag{20a}$$

$$J_z = -j\omega\epsilon_o \left(1 - \frac{\omega_{pi}^2 + \omega_{pe}^2}{\omega^2}\right) E_z \tag{20b}$$

$$U_z = -\frac{j}{\beta_p}\left[E_{z+} e^{j\beta_p z} - E_{z-} e^{-j\beta_p z}\right] e^{j(\omega t - \beta_e z)}. \tag{20c}$$

6. Two Infinite Parallel Planes, with Separation 2w Filled with Beam and Plasma

The dispersion equations are:

$$\frac{\tan \beta_{t1} w}{\tan \beta_{t2} w} = \frac{\beta_{t2,1}\left[\left(\beta_z^2 - k_1^2\right)\left(\beta_z^2 - k_1^2 + \beta_{t1,2}^2\right) - k_2^4 + \beta_z^2\left(\beta_z^2 + \beta_{t1,2}^2\right)\frac{\epsilon_4}{\epsilon_1}\right]}{\beta_{t1,2}\left[\left(\beta_z^2 - k_1^2\right)\left(\beta_z^2 - k_1^2 + \beta_{t2,1}^2\right) - k_2^4 + \beta_z^2\left(\beta_z^2 + \beta_{t2,1}^2\right)\frac{\epsilon_4}{\epsilon_1}\right]} \tag{21a}$$

with $\beta_{t1} \neq \beta_{t2}$, and

$$\beta_{t1,2}^4 - (a+c)\,\beta_{t1,2}^2 + ac - bd = 0. \tag{21b}$$

The longitudinal electric field is given by

$$E_2 = \left[C_1 \cos \beta_{t1} x + C_2 \cos \beta_{t2} x + C_3 \sin \beta_{t1} x + C_4 \sin \beta_{t2} x\right] \exp\left[i(\omega t - \beta_z z)\right] \tag{22}$$

If we consider the first subscripts of β_t in (21a), we find

$$C_2 = -\frac{\cos \beta_{t1} w}{\cos \beta_{t2} w} C_1 \qquad C_3 = C_4 = 0$$

and for the second subscripts,

$$C_1 = C_2 = 0 \qquad C_4 = -\frac{\sin \beta_{t1} w}{\sin \beta_{t2} w} C_3.$$

For some specific values of B_o Eq. 21a becomes indefinite. These values of B_o and the corresponding propagation constant can be found from

$$\beta_{t1} = \frac{m\pi}{2w} \qquad \beta_{t2} = \frac{n\pi}{2w}, \qquad \text{with } m + n = \text{even} \tag{23}$$

or

$$a + c = \frac{(m^2+n^2)\,\pi^2}{4w^2}$$

$$ac - bd = \frac{m^2 n^2 \pi^4}{16 w^4}.$$

7. Circular Waveguide (Radius R_o)

The dispersion equations for a completely filled circular, metallic waveguide are:

$$\beta_{t1}\left(qb+sc-s\beta_{t2}^2\right) \frac{J_n'(\beta_{t1}R_o)}{J_n(\beta_{t1}R_o)} - \beta_{t2}\left(qb+sc-s\beta_{t1}^2\right) \frac{J_n'(\beta_{t2}R_o)}{J_n(\beta_{t2}R_o)} = \frac{jnr}{R_o}\left(\beta_{t1}^2-\beta_{t2}^2\right) \tag{24}$$

and Eq. 21b. Then

$$E_2 = C_1\left[J_n(\beta_{t1}r) - \frac{J_n(\beta_{t1}R_o)}{J_n(\beta_{t2}R_o)} J_n(\beta_{t2}r)\right] \exp[j(n\phi+\omega t-\beta_2 z)]. \tag{25}$$

Again, for some specific values of B_o Eq. 24 becomes indefinite. The values of B_o and the corresponding propagation constant may be found from

$$a + c = \frac{a_{\ell n}^2 + a_{mn}^2}{R_o^2}; \quad ac - bd = \frac{a_{\ell n}^2 a_{mn}^2}{R_o^4} \tag{26}$$

where $a_{\ell n}$ and a_{mn} are the ℓ^{th} and m^{th} zeros of J_n.

8. Effects of Temperature

The fields and the dispersion equations can be determined in terms of the parameters p, q, r, s, t, u, a, b, c, d, which we have used in this treatment. When the plasma electrons have an initial temperature the above-mentioned parameters will remain the same functions of ϵ_1, ϵ_2, ϵ_3, ϵ_4, ϵ_5, but the temperature will change the elements

of the dielectric tensor.

The element ϵ_1 previously had the value

$$\epsilon_1 = \epsilon_o\left(1 + \frac{\omega_{pi}^2}{\omega_{ci}^2 - \omega^2} + \frac{\omega_{pe}^2}{\omega_{ce}^2 - \omega^2} + \frac{\omega_{pb}^2(\omega-\beta_z v_{ob})}{\omega\left[\omega_{cb}^2-(\omega-\beta_z v_{ob})^2\right]}\right).$$

Now, its value is

$$\epsilon_1 = \epsilon_o\left(1 + \frac{\omega_{pi}^2}{\omega_{ci}^2 - \omega^2} + \frac{\omega_{pe}^2}{\omega}\int \frac{f_e(u)(\omega-\beta_z u)\,du}{\omega_{ce}^2 - (\omega-\beta_z u)^2} + \frac{\omega_{pb}^2(\omega-\beta_z v_{ob})}{\omega\left[\omega_{cb}^2-(\omega-\beta_z v_{ob})^2\right]}\right). \tag{27}$$

For a square distribution $-u_o \leq u_e \leq u_o$ we find

$$\epsilon_1 = \epsilon_o\left(1 + \frac{\omega_{pi}^2}{\omega_{ci}^2 - \omega^2} + \frac{\omega_{pe}^2}{4\beta_z u_o \omega}\,\ell_n\left\{\frac{\omega_{ce}^2 - (\omega-\beta_z u_o)^2}{\omega_{ce}^2 - (\omega+\beta_z u_o)^2}\right\} + \frac{\omega_{pb}^2(\omega-\beta_z v_{ob})}{\omega\left[\omega_{cb}^2-(\omega-\beta_z v_{ob})^2\right]}\right).$$

In the same way we derive the expressions for ϵ_2, ϵ_3, ϵ_4, ϵ_5.

P. E. Serafim

References

1. P. E. Serafim, Interaction of an electron beam with plasma, Quarterly Progress Report No. 63, Research Laboratory of Electronics, M. I. T., October 15, 1961, pp. 15-21.

2. B. D. H. Tellegen, Philips Research Reports 3, 81 (1948).

3. A. A. Th. M. Van Trier, Appl. Sci. Research B3, 305 (1953).

F. HIGH-ENERGY CYCLOTRON RESONANCE OF ELECTRONS IN A PLASMA*

An experiment is being prepared to study cyclotron resonance of electrons in a plasma at high energy levels. Pulses of 1 Mw peak power, length 10 μsec, at a wavelength of 10 cm are obtained from a high power magnetron and delivered to a cylindrical cavity at resonance.

Another magnetron of lower power output is utilized in a continuous wave mode to

*This research was supported in part by Purchase Order DDL B-00306 with Lincoln Laboratory, a center for research operated by Massachusetts Institute of Technology with the joint support of the U.S. Army, Navy, and Air Force under Air Force Contract AF19(604)-7400.

pre-ionize the gas, and to study the discharge at low energy. A water-cooled magnet provides an axial magnetic field of intensity adjustable to make the cyclotron frequency of the electrons coincide with the frequency of the applied e.m. field. The cavity is connected to a vacuum system including a Vac Ion pump capable of obtaining a vacuum of the order of 10^{-7} mm Hg.

Future investigations may include studies of the resonance conditions for the cavity, the characteristics of the high energy discharge, and the attainment of high temperatures.

G. Fiocco

G. FIXED-FREQUENCY METHOD OF MEASURING PLASMA DENSITY*

In large plasma devices microwave optical methods are often used to measure the plasma density.[1,2] The interpretation of the microwave data, for example phase shift through the plasma, is generally based on four theoretical assumptions:

(a) That one can neglect the effects of the metallic walls of the plasma device, and base the interpretation on a free-space analysis (see Fig. XV-4);

(b) That the plasma geometry, usually a finite column, can be idealized as a slab, infinite in extent and finite in thickness;

(c) That the plasma slab is located in the far-field regions of the measuring horns; and

(d) that the reflections at the boundaries of the slab can be neglected.

Some experiments at Princeton[3] have shown that in a particular geometry the

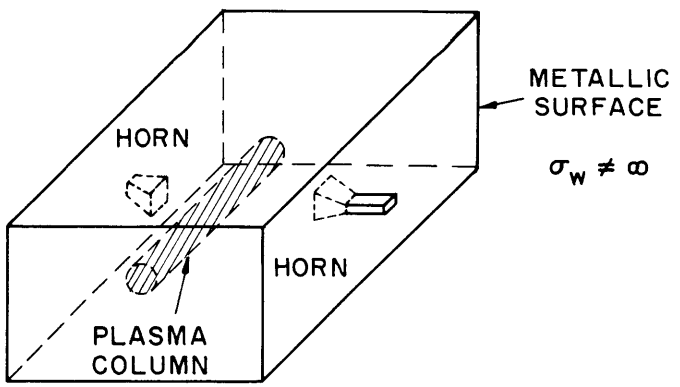

Fig. XV-4. Simplified drawing of a plasma device with horns for electromagnetic measurements.

*This research was supported in part by Purchase Order DDL B-00306 with Lincoln Laboratory, a center for research operated by Massachusetts Institute of Technology with the joint support of the U.S. Army, Navy, and Air Force under Air Force Contract AF19(604)-7400.

phase-shift data could be interpreted on the basis of an infinite plasma-slab model, if the actual diameter of the plasma column exceeded 3-4 wavelengths. Since not all experiments meet this requirement, and since it was not clear how the size and separation of the measuring antennas, and so forth affected this conclusion, we decided to study the finite geometry a little more generally.

Theoretical studies of the effects of removing assumption (b) have been reported.[4] If we try to remove both assumptions (b) and (c), we have integrals that are difficult to evaluate. In the interpretation of microwave data, if the finite size of the plasma and the near field of the horns are taken into account, we should also recognize the more important effects of the reflections from the metallic surfaces of the plasma device. The theoretical treatment of all of these effects leads to a re-examination of the problem of microwave measurement of plasma density in large plasma devices.

The analysis has led us to fixed-frequency method of measuring plasma density. The basic idea is to treat the enclosure of the plasma devices (since the walls of such devices are usually metallic surfaces) as a large microwave cavity. Since the densities achieved in these plasma devices are high, $n_o = 10^{13}$ to 10^{15} electrons per cubic centimeter, and since the single-frequency method requires operation at a frequency greater than the plasma frequency, the large microwave cavity may support millions of modes. In particular, the number of modes that are excited within a frequency range of Δf can be found from Eq. 1.

$$dN = 3N \frac{\Delta f}{f}, \tag{1}$$

where N is the total number of modes with characteristic frequencies that are less than the operating frequency. Thus, it is generally not possible to pick a single, isolated resonance of the system and find the perturbing effect of the plasma on this resonance. The average spacing of resonant modes in a large cavity is much less than the width of the average mode. With the present analysis we are able to use the change of impedance in a connecting waveguide, because of the presence of the plasma, to compute ω_p.

Assume a waveguide coupled to the cavity, and that only the dominant mode is propagated at the operating frequency. Then, at the input plane A in the waveguide, we can defined an impedance Z. (See Fig. XV-5.)

To determine plasma density from measurements of Z, we may use either of two approaches. The first is to expand the fields in the plasma device in terms of a set of orthonormal modes, satisfy boundary conditions, make some approximations, and arrive at a solution of $Z(n_o)$. This approach is tedious; it has been done but will not be reported on here.

A more elegant method is the perturbation technique that gives an identical expression for Z, and does not involve us in a maze of algebra. The perturbation technique

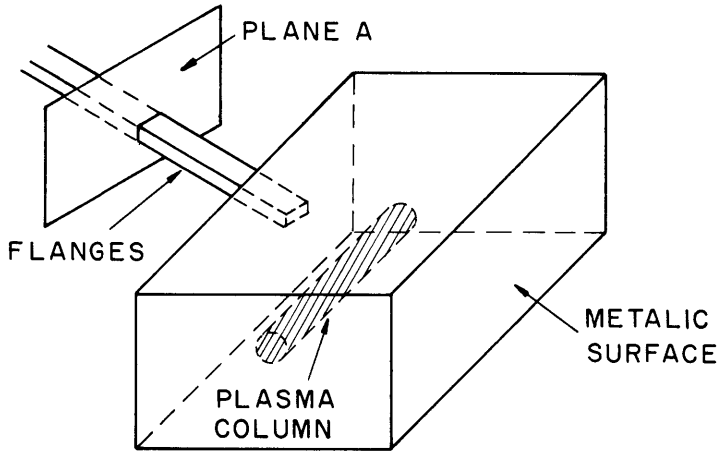

Fig. XV-5. Simplified drawing of a plasma device treated as a large microwave cavity.

treats both the plasma and the wall loss as perturbations of a hypothetical lossless cavity. The perturbation approach is based on two assumptions concerning the system that is being studied:

(i) $\omega\epsilon_o \ll \sigma_w$ (conductivity of the walls);

(ii) $\omega_p^2 \ll \omega^2$.

The hypothetical lossless cavity is defined as having perfectly conducting walls replacing the metallic surfaces, up to but not including plane A. Maxwell's equations for this cavity are:

$$\nabla \times \bar{E} = -j\omega\mu_o \bar{H} \tag{2}$$

$$\nabla \times \bar{H} = j\omega\epsilon_o \bar{E} \tag{3}$$

The boundary conditions are:

$$n \times \bar{E} = 0 \qquad \text{(over metallic surface)} \tag{4}$$

$$\bar{E} = \sum_{\ell} V_\ell \hat{e}_\ell \qquad \text{(sum of waveguide modes over plane A)} \tag{5}$$

If we make measurements at a plane that is an integral number of half-wavelengths from plane A, since all the higher-order modes decay, we only need to consider the dominant waveguide mode at plane A. Maxwell's equations for the plasma device, in which wall loss and plasma are treated as perturbations, are

$$\nabla \times \delta\bar{E} = -j\mu_o \delta(\omega\bar{H}) \tag{6}$$

$$\nabla \times \delta\bar{H} = j\epsilon_o \delta(\omega\bar{E}) + \bar{J}_p \tag{7}$$

$$\bar{J}_p = -j\omega\epsilon_o \frac{\omega_p^2}{\omega^2} \bar{\bar{K}}_p \cdot \bar{E} \tag{8}$$

and the boundary conditions are

$$\delta\bar{E} = -\sqrt{\frac{\omega\mu_o}{2\sigma_w}}\,(1+j)(\bar{n}\times\bar{H}) \qquad \text{(over metallic surface)} \tag{9}$$

$$\delta\bar{E} = \delta V_{10}\hat{e}_{10} \qquad \text{(over plane A)} \tag{10}$$

It is assumed that the plasma is electrically neutral and that only the electrons respond to the electric field; the ions are assumed to be stationary. Since we have assumed $\omega_\rho^2 \ll \omega^2$, we also assume that the electric field acting on electrons is that which would exist in the empty cavity (space-charge fields are ignored). The resultant expression for the susceptibility of the plasma, except for its negative sign, might apply to a dielectric material.

We can manipulate Eqs. 2-10 to obtain an expression for the change of the impedance measured in the driving waveguide at constant frequency. This expression is

$$\delta Z = \frac{1}{|I_o|^2}\left\{(1+j)\sqrt{\frac{\omega\mu_o}{2\sigma_w}}\int_{\substack{\text{cavity}\\\text{wall}}} \bar{H}\cdot\bar{H}^*\,ds + \int \bar{J}_p\cdot\bar{E}^*\,dv\right\}. \tag{11}$$

Equation 11 shows that in the first-order perturbation theory, the effects of the perturbation are additive. Our use of Eq. 11 will be limited to a weak, homogeneous, and isotropic plasma ($\omega_\rho \gg \omega_c$).

We now make a series of measurements which by a calibration method accounts for the effect of the finite size of the plasma and for the losses in the metallic surfaces.

In the absence of the polarization currents the impedance seen at plane A is

$$Z_1 = Z + \frac{1}{|I_{10}|^2}\sqrt{\frac{\omega\mu_o}{2\sigma_w}}\,(1+j)\int_{\text{wall}} \bar{H}\cdot\bar{H}^*\,ds. \tag{12}$$

The impedance Z denotes the contribution from the lossless cavity. The separation in Eq. 12 is a mathematical convenience, and the physical quantity that can be measured is the complex value of Z_1 at the arbitrary plane A.

The impedance of the cavity with the plasma is

$$Z_2 = Z_1 - j\omega\epsilon_o \frac{\omega_p^2}{\omega^2}\int_{\text{plasma}} \bar{E}\cdot\bar{E}^*\,dv\,\left(1 + j\frac{\nu_c}{\omega}\right). \tag{13}$$

Then, Z is measured with a dielectric material of a known dielectric constant, $(\epsilon/\epsilon_o - 1) < 1$, and of the same geometrical shape as the plasma column placed in the cavity, with the result that

$$Z_3 = Z_1 + j\omega\epsilon_o\left(\frac{\epsilon}{\epsilon_o} - 1\right) \int \bar{E} \cdot \bar{E}^* \, dv. \tag{14}$$

Finally,

$$\frac{\omega_p^2}{\omega^2} = \left(\frac{\epsilon}{\epsilon_o} - 1\right) \frac{\mathrm{Im}[Z_1 - Z_2]}{\mathrm{Im}[Z_3 - Z_1]}.$$

The fixed-frequency method of measuring plasma density has replaced the free-space optical assumptions by another set of assumptions that are noted throughout this report. In addition, in the calibration measurements we make rather stringent assumptions about the plasma. It is assumed that the plasma is in the form of a rod with a uniform distribution inside the rod and zero distribution outside. Also, it is assumed that the plasma diameter is known and that its position in the cavity is known.

H. Y. Hsieh

References

1. R. F. Post, T. F. Prosser, and C. B. Wharton, Microwave Diagnostics in Arc Research, Report UCRL 4477, University of California, 1958.

2. M. A. Heald, The Application of Microwave Techniques to Stellerator Research, Report MATT 17, Princeton University, August 26, 1959.

3. B. Rosen, The Inverted Universe Plasma Analog for Microwaves, Technical Memorandum No. 85, Project Matterhorn, Princeton University, August 18, 1959.

4. H. Y. Hsieh, Scattering of waves by a tenuous plasma of finite geometry, Quarterly Progress Report No. 62, Research Laboratory of Electronics, M.I.T., July 15, 1961, pp. 52-56.

H. PROBE MEASUREMENTS IN THE HOLLOW-CATHODE DISCHARGE*

1. Introduction

In an earlier report[1] Langmuir probe measurements in the hollow-cathode discharge were described and interpreted according to the simplest probe theory. A Maxwellian

*This research was supported in part by Purchase Order DDL B-00306 with Lincoln Laboratory, a center for research operated by Massachusetts Institute of Technology with the joint support of the U.S. Army, Navy, and Air Force under Air Force Contract AF19(604)-7400.

distribution was assumed for the plasma electrons, and the effect of the magnetic field was ignored. A symmetric probe was used, so that the anisotropic nature of the electron distribution could not be investigated.

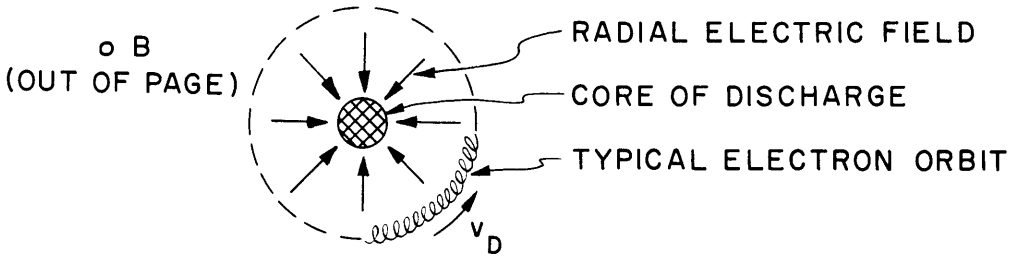

Fig. XV-6. Drift motion of electrons in cylindrical geometry, caused by crossed electric and magnetic fields.

The plasma in the hollow-cathode discharge is confined by a strong magnetic field that reduces the electron Larmor radius to a fraction of 1 mm. Radial electric fields, caused by space-charge separation, often exist in a cylindrical discharge configuration. In the presence of crossed electric and magnetic fields, all of the charged particles (regardless of their mass and charge) acquire a drift velocity (see Fig. XV-6)

$$\vec{V}_D = \frac{\vec{E} \times \vec{B}}{|B|^2} . \tag{1}$$

However, a particle starting from rest must travel a distance that is comparable to a cyclotron radius before it attains this velocity. Because the ion cyclotron radius is greater than the dimension of the apparatus, the drift velocity will not be observed for ions. Electrons, on the other hand, travel a very short distance before acquiring this drift velocity. Hence, one should expect to observe a drift current of electrons in the azimuthal direction, whose density is

$$J_D = \frac{eNE}{B} , \tag{2}$$

where N is the electron density in the plasma.

Since the magnetic field B is easily measurable, Eq. 2 suggests that either E or N could be determined by measuring J_D.

If the electric field E is to be determined, N can be calculated from the random ion current density (obtainable from the probe characteristic) according to Bohm's formula[2]

$$N = \frac{J^+}{0.4e\sqrt{\frac{2eV_T}{m_+}}} , \tag{3}$$

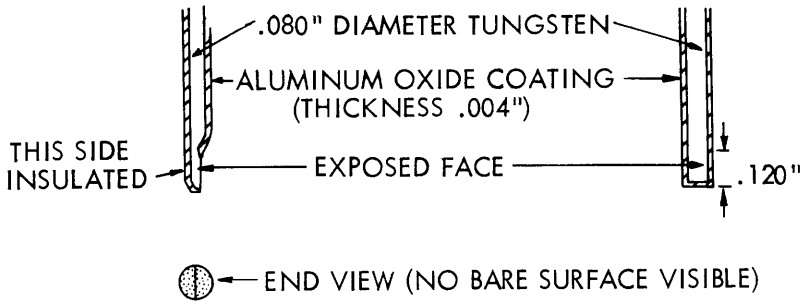

Fig. XV-7. Unidirectional plane probe.

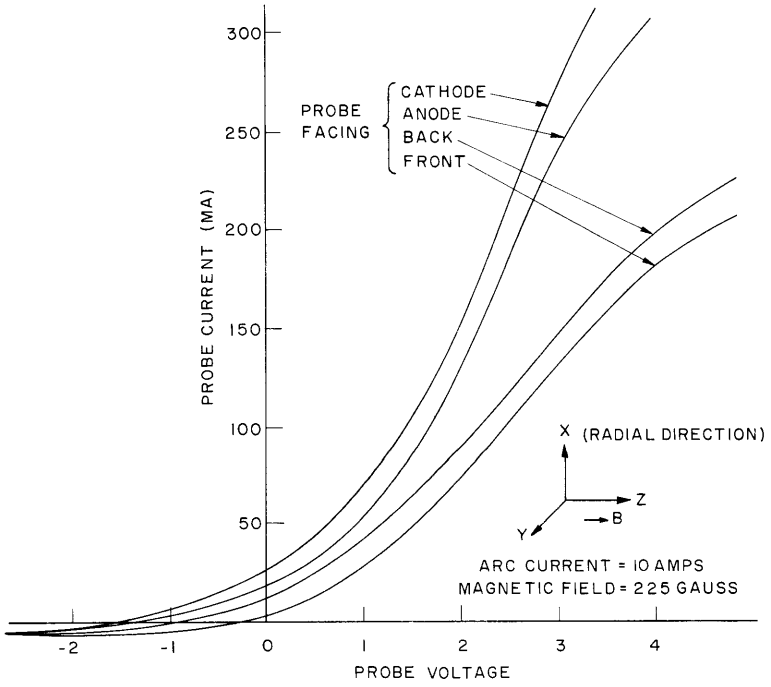

Fig. XV-8. Characteristics obtained by rotating the plane probe of Fig. XV-7. The magnetic field is pointed toward the anode, so that, if the coordinate system of Fig. XV-7 is used, "front" represents the positive y-direction; "back," the negative y-direction; "anode," the positive z-direction, etc.

where V_T is the electron temperature in volts. It has been shown by Bohm, Burhop, and Massey[2] that this formula is applicable even in the presence of the magnetic field.

If the electron density N is to be calculated from Eq. 2, then the radial electric field can be determined by using a movable probe to measure plasma potential as a function of radial position.

In order to demonstrate the use of Eq. 2, a probe was constructed which collected electrons from only one direction. The end of a tungsten rod was ground to the shape illustrated in Fig. XV-7. All of the surface, except for the plane conducting surface, was covered with a 0.1-mm coating of aluminum oxide. The "plane probe" could be turned to face in the transverse or longitudinal directions, but not in the radial direction. The dimensions of the collecting face (2 × 3 mm) were of the order of several electron Larmor radii.

2. Experimental Results

The plane probe was held in a fixed radial position and rotated to face in each of the four directions (toward the cathode, toward the anode, and in the "front" and "back" transverse directions). The probe characteristic was recorded for each direction. One of the sets of curves obtained in this manner is shown in Fig. XV-8.

When the probe was rotated the full 360°, the electron current exhibited two maxima (in the two longitudinal directions) and two minima (in the two transverse directions). Before each curve was recorded, the probe was carefully adjusted to collect the appropriate maximum or minimum current. The ion current showed no dependence on direction, which result lends support to the validity of Eq. 3, even in the presence of a strong magnetic field.

The curves show that the electrons have drift velocities from cathode to anode and from "front" to "back" in the transverse direction. When the magnetic field was reversed, the "front" and "back" curves exchanged, while the "anode" and "cathode" curves remained unaltered.

For either direction of the magnetic field, the transverse drift current could be explained by the $\vec{E} \times \vec{B}$ drift velocity, provided that the electric field pointed toward the axis of the discharge. The measurements of plasma potential verified the fact that the radial electric field did indeed point inward.

The elementary probe theory was applied to obtain the plasma potential as a function of radial distance from the axis of the arc,[3] as shown in Fig. XV-9. Both positive and negative plasma potentials (with respect to the anode) were observed, but these observations depended upon the various arc parameters. The electric field, however, always pointed inward. When positive plasma potentials were observed, a potential maximum must have occurred between the arc axis and the chamber wall (which was at anode

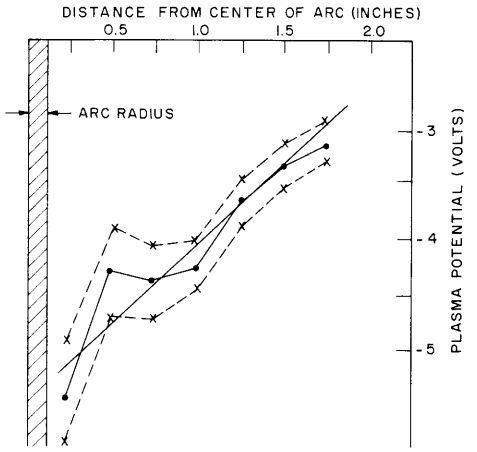

Fig. XV-9. Variation of plasma potential with radial position in a magnetic field of 300 gauss. The dashed lines indicate the estimated error in measuring V_s from probe curves. The straight line has a slope of 60 volts per meter. The probe curves were made with the plane probe facing in the transverse direction

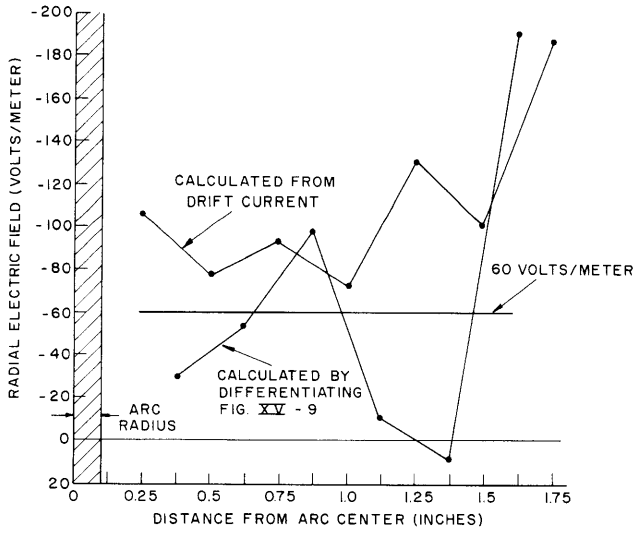

Fig. XV-10. Variation of radial electric field with position, calculated by two methods.

potential). No such maximum could be found in the range over which the probe could be moved, an indication that the maximum occurs very close to the wall. It is probable that a positive charge exists on the inner surface of the chamber wall.

It can be shown[3] that the difference in current density which is picked up in the two transverse directions is just equal to J_D, provided that the probe is at the plasma potential.

The electric field calculated from the drift current (by means of Eq. 2) is plotted in Fig. XV-10 in which it is compared with the field obtained by differentiating the plasma-potential curve of Fig. XV-9. Because the error in estimating the plasma potential from the probe curves is often larger than the difference in potential between two neighboring positions, it is almost hopeless to try to calculate the point-by-point variation of the radial electric field from the derivative of the curve in Fig. XV-9. The drift-current method gives at least a rough idea of the variation of E with radial position, and it could even be differentiated to give an average net charge density. By measuring J_D at smaller intervals, and by refining the probe and auxiliary equipment, we may be able to obtain better results, although there are many considerations, both practical and theoretical, which limit the accuracy of this technique. Among them are: (a) disturbance of the plasma by the probe; (b) fluctuations of the discharge itself during the time required to obtain a set of probe curves; (c) fringe effects around the edges of the collecting face; and (d) error in measuring electron temperature and density.

These and other problems, along with several other applications of the one-sided plane probe, are discussed in the author's thesis.[3]

A. W. Starr

References

1. A. W. Starr, Probe measurements in the hollow-cathode discharge, Quarterly Progress Report No. 61, Research Laboratory of Electronics, M. I. T., April 15, 1961, pp. 40-43.

2. A. Guthrie and R. K. Wakerling, Characteristics of Electrical Discharges in a Magnetic Field (McGraw-Hill Book Company, Inc., New York, 1949), Chapter 2.

3. A. W. Starr, Probe Measurements in the Hollow Cathode Arc, S. M. Thesis, Department of Electrical Engineering, M. I. T., August 1961.

I. LARGE-SIGNAL ELECTRON-STIMULATED PLASMA OSCILLATIONS*

Certain properties of large-signal plasma oscillations have been studied with basically the same apparatus described[1] in Quarterly Progress Report No. 61. The

*This research was supported in part by Purchase Order DDL B-00306 with Lincoln Laboratory a center for research operated by Massachusetts Institute of Technology with the joint support of the U.S. Army, Navy, and Air Force under Air Force Contract AF19(604)-7400.

beam-plasma interaction region and the instrumentation are shown schematically in Fig. XV-11. In this experiment an electron beam was injected from a magnetically shielded electron gun into the electric field-free drift tube shown in Fig. XV-11. The vacuum system, which has been described previously,[2] maintains a pressure of 10^{-5} mm Hg in the gun region, and from 10^{-4} to 10^{-3} mm Hg of argon in the drift tube.

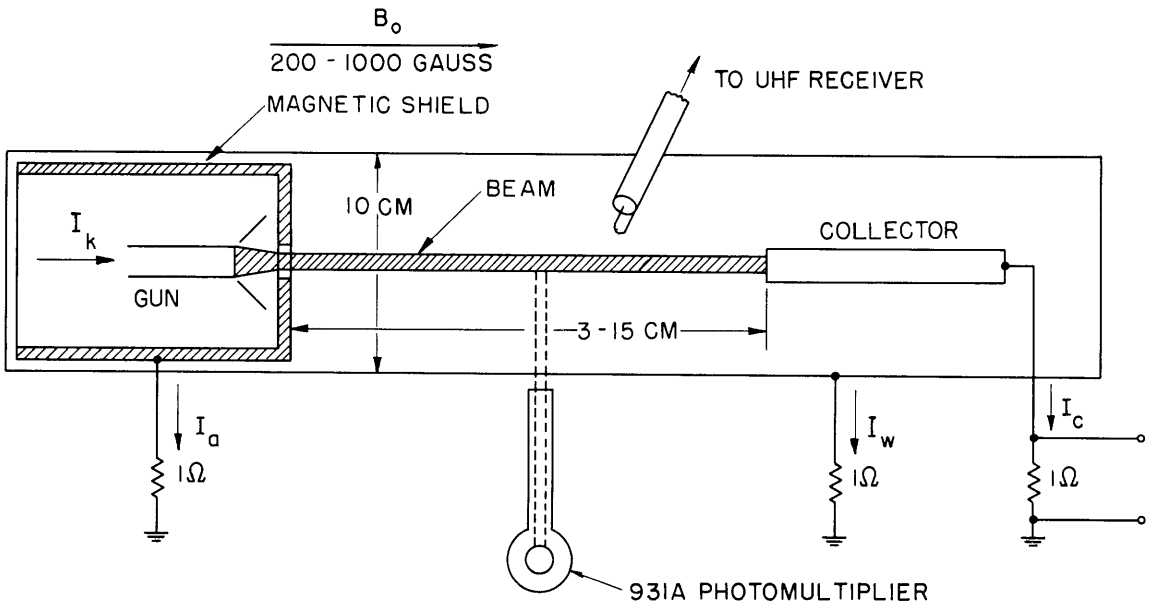

Fig. XV-11. Drift-tube region for the beam-generated plasma experiment. (Beam characteristics: $I/V^{3/2} = 10^{-6}$ (10 kv, 1 amp); Beam diameter: ~0.08 inch; Pulse duration, 3.5 μsec; Pulse repetition rate, 50-500/sec.)

As previously described, the flow of beam current to the collector is disrupted by plasma oscillations that start 1-2 μsec after the beam pulse is turned on. When the oscillations start a sharp break occurs in the collector current (I_c), and the missing current turns up in the drift-tube wall current (I_w). The electron beam is scattered to the walls by the rf electric fields that appear in the drift tube simultaneously with the decrease in collector current. These rf oscillations are excited by noise in the beam and beam-generated plasma, and amplified by the interaction between slow waves propagating along the beam and in the plasma.

The small-signal theory predicts amplification at frequencies at which the beam and plasma waves are synchronous.[3] There are two regions of synchronism that are of interest, and these are in the frequency range $f_c < f < \left(f_c^2+f_{pp}^2\right)^{1/2}$ when $f_{pp} < f_c$, and $f_c < f < \bar{f}_{pp}$ when $f_{pp} > f_c$, where f_{pp} is the plasma frequency of the beam-generated

plasma, f_c the electron-cyclotron frequency, and $\bar{f}_{pp}$ is a frequency slightly greater than f_{pp}. The first of these is the region in which the slow cyclotron wave of the beam is synchronous with a backward wave in the plasma, with resulting backward-wave amplification or oscillations analogous to the beam-circuit interaction in a backward-wave oscillator.[4] In the second region, the conditions are such that reactive-medium amplification 3 can occur, and thus produce a large amplification near f_{pp}. Since the plasma is generated by the beam, the plasma density continually increases with time as long as the beam current flows. For this reason, we expect that if the oscillations start when noise is amplified by reactive-medium amplification, the first observable signal will increase with time as f_{pp} increases. On the other hand, if the oscillations start before f_{pp} reaches f_c, the backward-wave amplification will be dominant and the frequency of the first observable signal will lie between f_c and $\left(f_c^2+f_{pp}^2\right)^{1/2}$.

In our studies of the rf spectrum, a receiver that is tunable from 10 mc to 4.5 gc, and has an output video bandwidth of approximately 2.5 mc was used. With this receiver, we could measure the delay time between the initial rise of the beam and the beginning of the rf pulse at any frequency in the tuning range. The frequency of the rf pulse with the smallest delay presumably lies in the frequency range of the small-signal interaction that is dominant during the build-up of the rf field. We measured the frequency of this minimum-delay rf pulse, which we shall refer to as the "precursory signal," as a function of magnetic flux density over a 3.5-1 range of the field. For a wide range of the operating conditions (determined specifically by the beam voltage, beam current, pressure of argon, and length of drift tube), we found that the precursory-signal frequency is proportional to and slightly greater than f_c, the electron-cyclotron frequency. This result indicates that the oscillations are started by the backward-wave interaction, which occurs between f_c and $\left(f_c^2+f_{pp}^2\right)^{1/2}$, and that at the starting time the plasma frequency is less than f_c. An example of the variation of the precursory-signal frequency with f_c is shown in Fig. XV-12.

The precursory signal was a small fraction of the complete rf spectrum. From a spectrum analysis at a fixed f_c, we found that an almost continuous spectrum was generated from 100 mc to 800 mc (approximately f_c) at a time slightly later than the starting time of the precursory signal. Other signals were found at higher frequencies at later times.

By considering the process of plasma build-up we have concluded that in most cases (each point in Fig. XV-12, for example) the oscillations start when f_{pp} is less than f_c. As discussed below, the oscillations increase the rate of plasma generation, and f_{pp} soon exceeds f_c. At a later time, therefore, the required condition, $f_{pp} > f_c$, for reactive-medium amplification is satisfied. It is possible that the frequency of an amplified signal occurring at this time will be f_{pp}, and this frequency will increase as time goes on. Signals could be found with this characteristic, but sufficiently consistent operation could

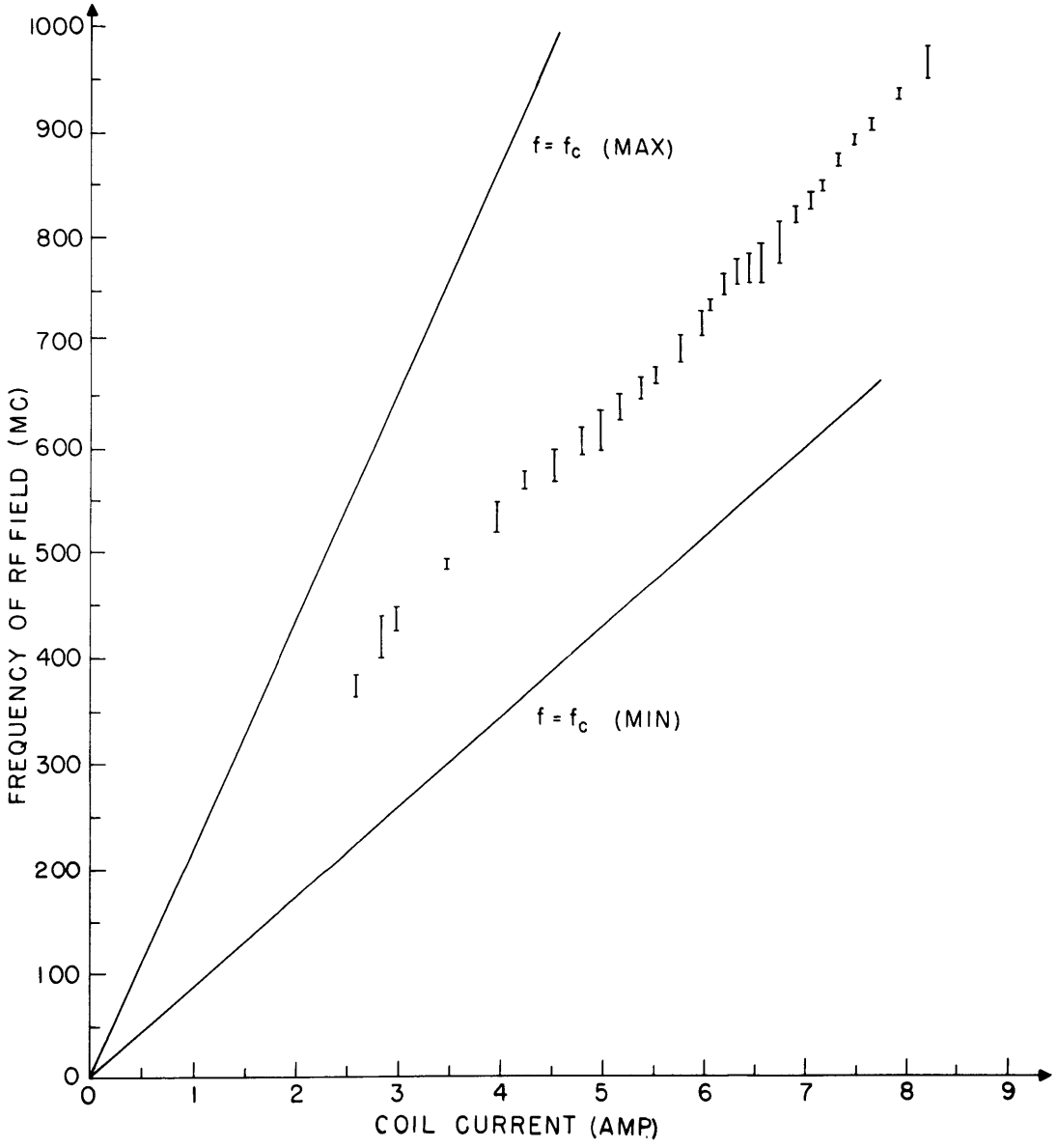

Fig. XV-12. Variation of the frequency of the precursory signal with coil current. The lines indicated by f_c(max) and f_c(min) indicate the range of f_c along the beam length at each value of coil current.

not be obtained to provide quantitative results.

Several modes with different angular dependencies of the fields are predicted by the small-signal theory[3] in the range $f_c < f < \left(f_c^2+f_{pp}^2\right)^{1/2}$. Considering the fact that a transverse ac electric field is necessary for scattering the beam across the axial dc magnetic field, we expect that the n = 1 mode is excited because this mode has such a field and thereby produces off-axis ac motion of the center of gravity of the beam. Experiments were performed to determine the fate of the scattered beam electrons by placing a circular, flat plate at the end of the collector tube which covered the total cross-section area of the drift tube. It was found that the beam is completely scattered to the drift tube (10-cm diameter) before it strikes the collector plate (14 cm from gun anode). The ac electric field amplitude required to produce this deflection is several thousand volts per centimeter.

Another phenomenon observed in this experiment is an effective heating of the plasma electrons. Scintillation measurements with Willemite-coated probes were made to detect heating effects. This phosphor has a luminescence threshold energy of approximately 100 ev. Our results indicate that electrons are accelerated to energies of at least 100 ev. In this energy range, the cross sections for ionization and excitation are both much larger than the cross sections for the beam electrons (10,000 ev), and the rate of ionization and excitation is increased. A large increase in the light emission from the discharge occurs as the result of an increase in the number of plasma electrons and/or an increase in the rate of excitation. This agrees with the results of our experiment, in which we found that the peak light intensity after the oscillations begin grows to 100 times the intensity of the light emitted before the oscillations start.

From these observations, we conclude that under certain operating conditions, the rf oscillations start at frequencies near the cyclotron frequency. The curves of Fig. XV-12 is the result obtained under typical operating conditions. The small-signal amplification mechanism that occurs in this frequency range is analogous to the beam-circuit interaction in a backward-wave oscillator or amplifier. The rf electric field causes scattering of the beam and acceleration of plasma electrons to energies of 100 ev, or more.

W. D. Getty

References

1. L. D. Smullin and W. D. Getty, Large-signal electron-stimulated plasma oscillations, Quarterly Progress Report No. 61, Research Laboratory of Electronics, M. I. T., April 15, 1961, pp. 33-36.

2. W. D. Getty and L. D. Smullin, Experimental results of the study of the hollow-cathode discharge, Quarterly Progress Report No. 58, Research Laboratory of Electronics, M. I. T., July 15, 1960, pp. 35-41.

3. L. D. Smullin and P. Chorney, Propagation in Ion-loaded Waveguides, Microwave Research Institute Symposium Series, Vol. VIII (Polytechnic Institute of Brooklyn, New York, 1958), p. 242.

4. D. L. Morse, Plasma Heating by the Electron Beam-Plasma Interaction, S. M. Thesis, Department of Electrical Engineering, M. I. T., 1960.

J. INVESTIGATION OF SUPERCONDUCTING TRANSITION OF Nb-Zr ALLOYS

As soon as they were discovered,[1] the Nb-Zr alloys appeared to be the most suitable superconducting material for our large-volume superconducting solenoid.[2, 3] These alloys are able to sustain fields up to 60-70 kgauss, and, moreover, they are ductile alloys with high strength: 250,000 psia yield point.[4, 5] Consequently, their utilization is much easier than that of the intermetallic type of superconductor, such as Nb_3Sn,[6] Nb_3Al or V_3Ga.

It has been most fortunate that the delicate processing of the wire was solved in a relatively short time, so that it is now a commercially available product.[7] We received our first short-length sample at the end of July 1961, and a long-length sample at the beginning of September 1961. Now, single lengths of up to 9000 ft have been produced.[8]

As soon as samples were received, determination of the superconducting transition curve was made in close collaboration with Dr. S. H. Autler of Group 82 of Lincoln Laboratory, M. I. T. We report here the results of this test.

1. Superconducting Transition

The superconducting transition experiment is carried out by a resistive method — the same, in principle as that described in connection with our study[9] on niobium wire. However, because of the magnitude of the field that is now required, the external field is provided by either the 4-inch, 67 kgauss or the 2-inch, 88 kgauss Bitter solenoid of the National Magnet Laboratory. Also, since the current is very high, the superconducting-to-normal transition is very sharp and results in a drastic reduction of the current; therefore, no voltmeter is necessary to determine the transition. Experiments have been made with only direct current drawn from a battery tank, and with the direction of the field always perpendicular to the direction of current. The results are shown as a plot of the critical current versus the applied field.

Our purpose was to determine and investigate the parameters that are of importance and of interest. They appear to be quite numerous, and this adds to the complexity of interpreting the experimental results. Our data are presented according to the different parameters studied, which are most logical and easier to understand.

We have chosen for this purpose some of our typically good results for the particular

parameters presented. It should not be overlooked that, in practice, all of the parameters play a role simultaneously, and the situation is not clear, as the curves show.

a. Effect of Connection

Figure XV-13 illustrates our point, since it refers to the same wire and to the same apparatus, but with various connections of the superconductor to the normal conductor that brings the electric current from the internal source.

Curves 1 and 2, with a current limited in the low-field, high-current region, seem to be typical of poor connections, and not at all of the intrinsic properties of the wire.

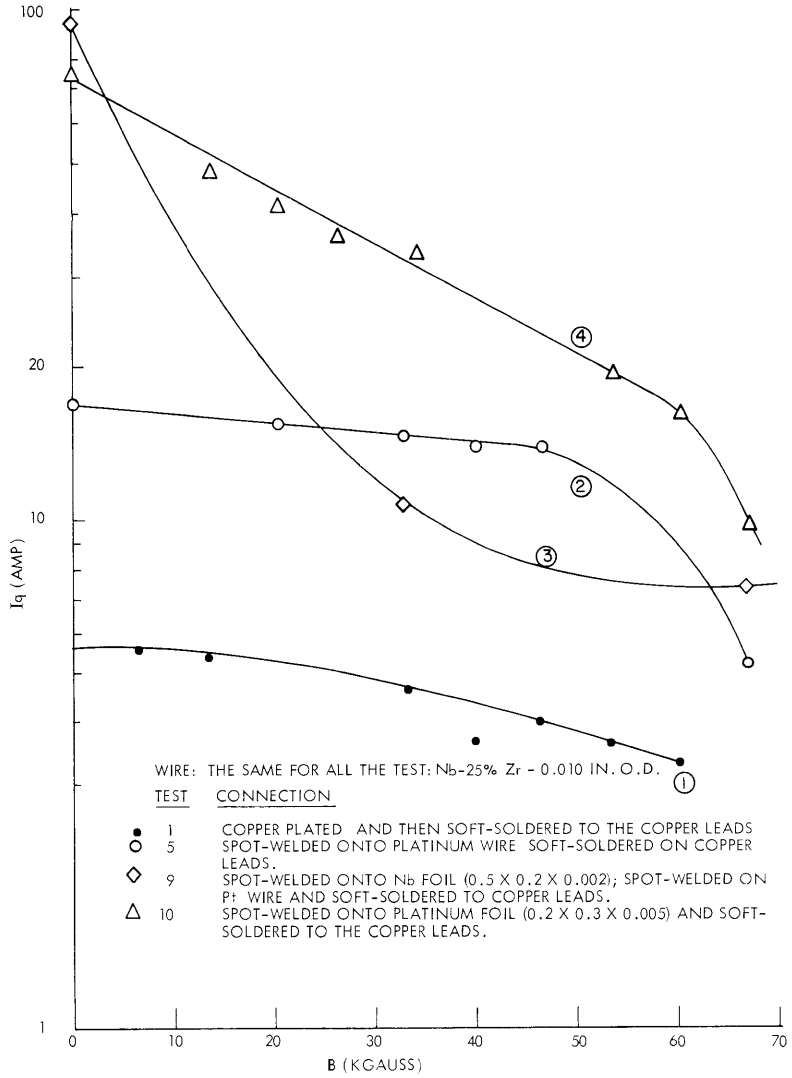

Fig. XV-13. Effect of superconductor connections to normal conductor on the transition curve I_c vs B (T=4.2°K).

Curves 3 and 4 seem to indicate a good contact. Note that the type of connection does not seem to be too relevant, since, for instance, "good-contact" curves were obtained later when an Nb clamp was used.

From all of our data, it appears that good contact is obtained by using: (a) a clean oxide-free extended surface (sandpaper cleaning just before making the connection seems to be sufficient); and (b) a large cross section of the normal material in the vicinity of the contact.

The basic cause of the current limitation is not clear, but this may well be due to local microscopic heating at the boundary of the superconducting region and

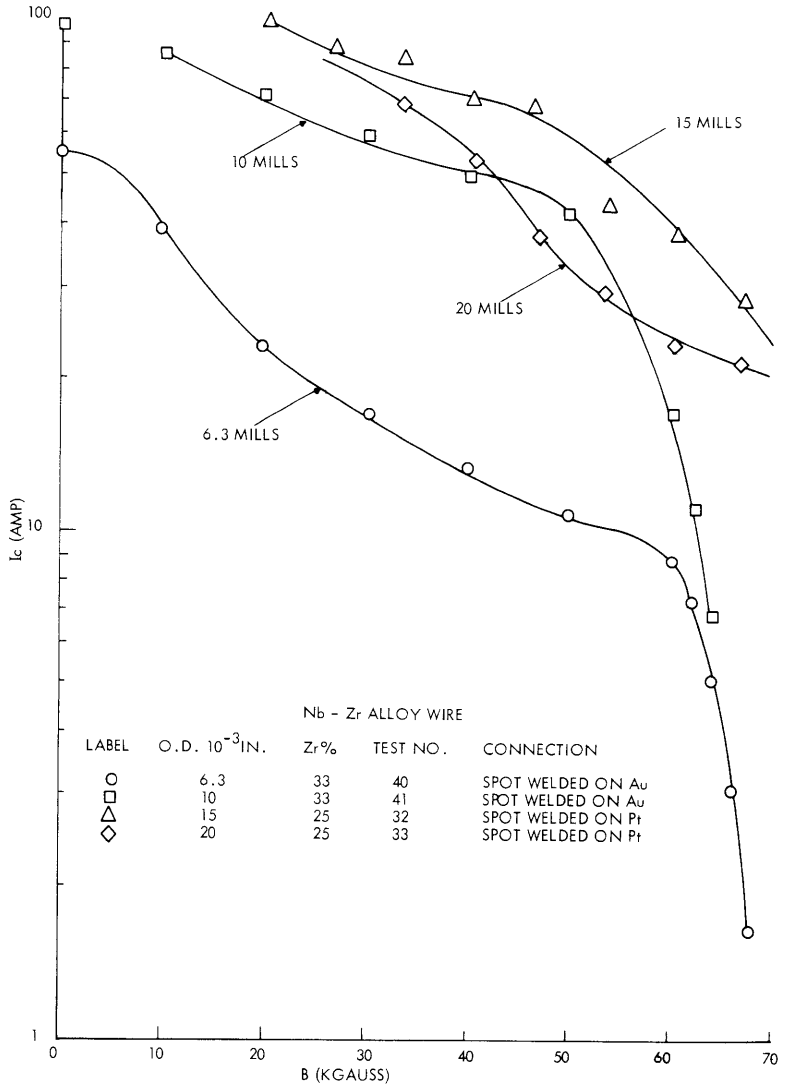

Fig. XV-14. Effect of the size of the wire on the transition curve I_c vs B (T=4.2°K).

normal conducting region, which impairs the production of the electrons into the superconducting state.

b. Effect of the Wire Size

Some typical results for sizes between 0.0063 in. and 0.020 in. are shown in Fig. XV-14. Observations above 100 amps were limited by the current supply available. For purposes of comparison, we have plotted the current density in Fig. XV-15. The 6.3-mil wire was obtained by further drawing of the 10-mil wire lot. The alloy is 33 per cent zirconium, whereas for the 15-mil and 20-mil it is 25 per cent zirconium. We think

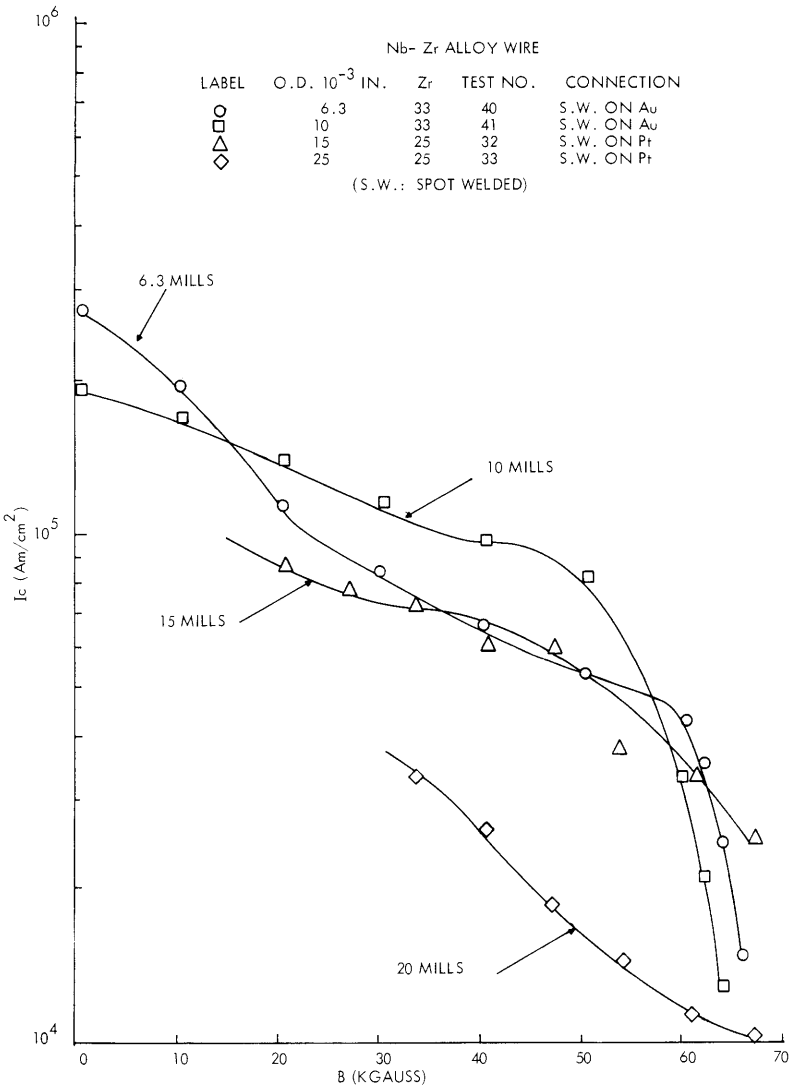

Fig. XV-15. Effect of the size of the wire on the current-density transition curve I_c vs B (T=4.2°K).

this does not invalidate the comparison because the composition in this range seems to have little effect on the characteristic curve.

The interpretation is quite involved, since all of the history of the wire comes into play, particularly cold-work and phase separation resulting from the heat treatment. However, it seems from the current density curve that the 20-mil wire is radically different from the others. This may be due to insufficient cold-work, although the amount of cold-work is quite large. It is more plausible that this indicates that a kind of threshold of cold-work is necessary to optimize the current-carrying capacity of a wire.

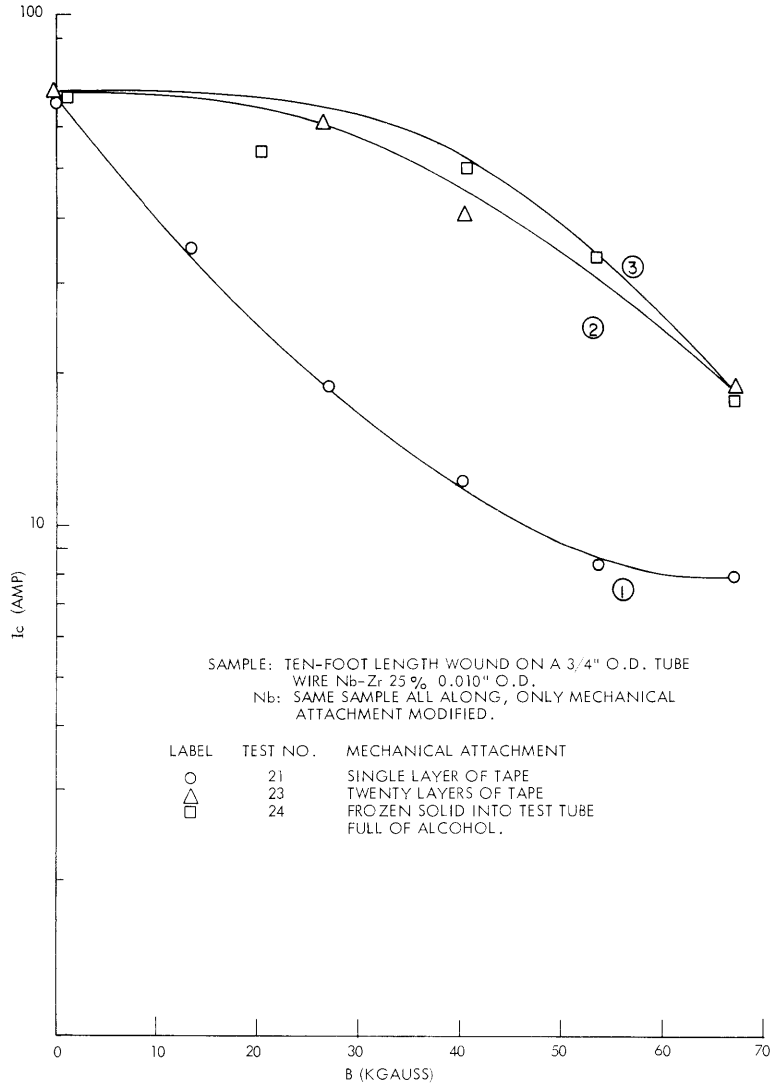

Fig. XV-16. Effect of the mechanical attachment of the sample on the transition curve I_c vs B (T=4.2°K).

c. Effect of the Mechanical Attachment of the Wire

The experiment to determine this effect, in which the same sample, including its connections, was used, was undertaken originally to study the effect of the heat transfer to the helium. We expected that the critical current would have been decreased by decreasing the heat-transfer coefficient between the wire and the helium bath. The results, as shown in Fig. XV-16, are the opposite. This indicates that the heat transfer to the helium is not by any means at fault, since the most thermally insulated wire has the highest critical current.

We think that the parameter that is at fault is the mechanical attachment of the wire to its support. To clarify this concept, the following experiment was devised. A string is attached to a short sample. When the superconducting current is established, a small pull of the string quenches it instantaneously, even with a very small current and no field. Indeed, although the wire is able to carry more than 100 amps with no field, a 1-mm pull wire it carries 1 amp quenches it immediately. This certainly proves that mechanical deformation of a superconducting wire carrying current is a first-order effect.

We can now explain the results of Fig. XV-16 in the following way. The Bitter magnet vibrates because of the water flowing through it. Our dewar is on top of it, and therefore the samples studied are also submitted to some vibrations. We think that the tightening reduces the vibrations of the wire and therefore limits the mechanical motion effect.

The basic cause of this phenomenon is not clear, but we think that this may be a heating effect at the microscopic level. Indeed, mechanical deformation involves friction and therefore heat generation. Although the amount of heat is small, the local temperature increase may be enough to reach the critical temperature, because of the extremely low specific heat of the solid material at 4.2°K. Also, the electrical work $j \times B$ may contribute sensibly to the heat-generating process beyond the friction itself, if a two-fluid model of the superconducting current is assumed.

d. Heat Treatment

Recent studies[10, 11] have shown that heat treatment during the processing improves the quality of Nb-Zr alloy wire. This improvement is much more sensitive for material of poor quality, and becomes comparable to that of good-quality wire. The manufacturer has applied such heat treatment to wires, and Fig. XV-17 shows the results. For comparison, we have also indicated the transition curve for a non heat-treated wire designated as standard and an annealed wire. The outcome seems quite discouraging, since the standard wire, which is not heat-treated, showed the best result. Let us say,

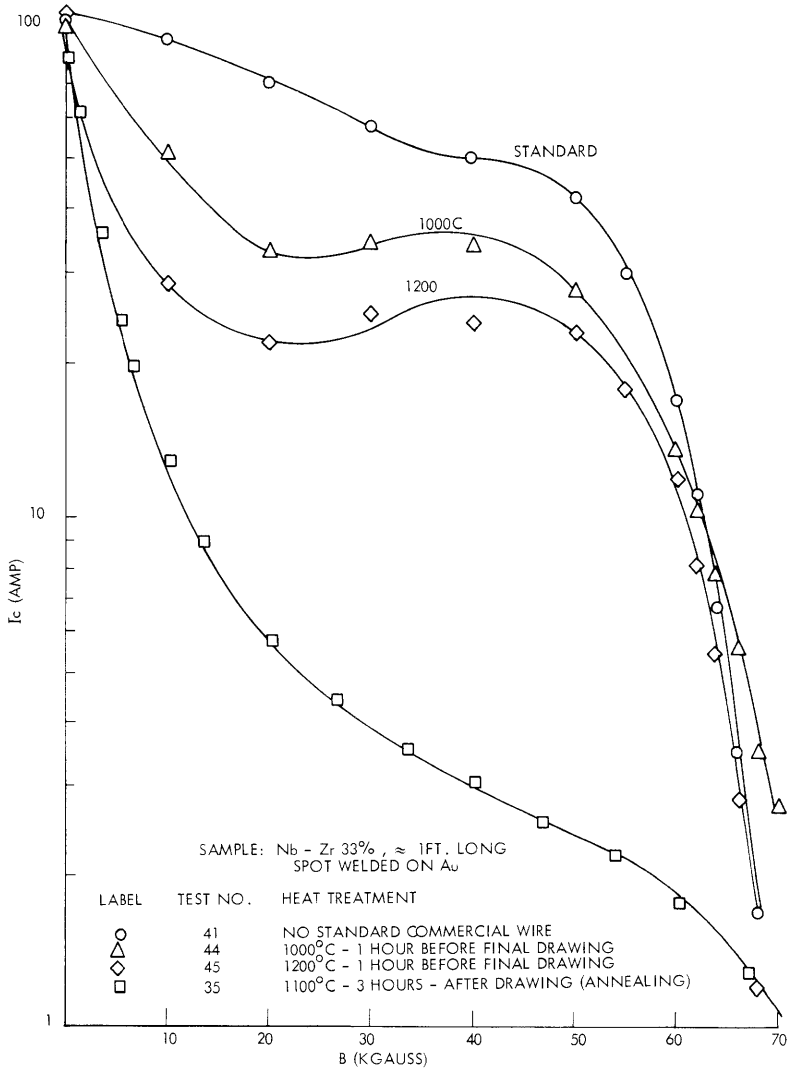

Fig. XV-17. Effect of the heat treatment on the transition curve I_c vs B (T=4.2°K).

however, that the heat treatment is not yet optimized and, as we shall show, the effect on the current capacity of a solenoid made of such wire may be quite different.

e. Comparison of the Transition Curves of a Small Solenoid and Short Samples

Figure XV-18 indicates clearly that the transition curves for short samples (less than 15 ft) and small solenoids are not similar. The difference is particularly large for the low-field high-current region of the curves, but the curves converge in the high-field region. The critical current of all of the solenoids in which Nb-Zr is used which have been made, thus far, seems to support the results of our experiments. This value is in the vicinity of 20 amps (±10 per cent) for a 10-mil wire having zirconium content between

20 per cent and 40 per cent. The corresponding current density is approximately 40,000 amps/cm^2. Surprisingly enough, we have found that solenoids made here before, either with 4-mil Nb wire or 3-mil Mo-Re of 40 per cent weight, also support a current density of approximately the same amount.[12]

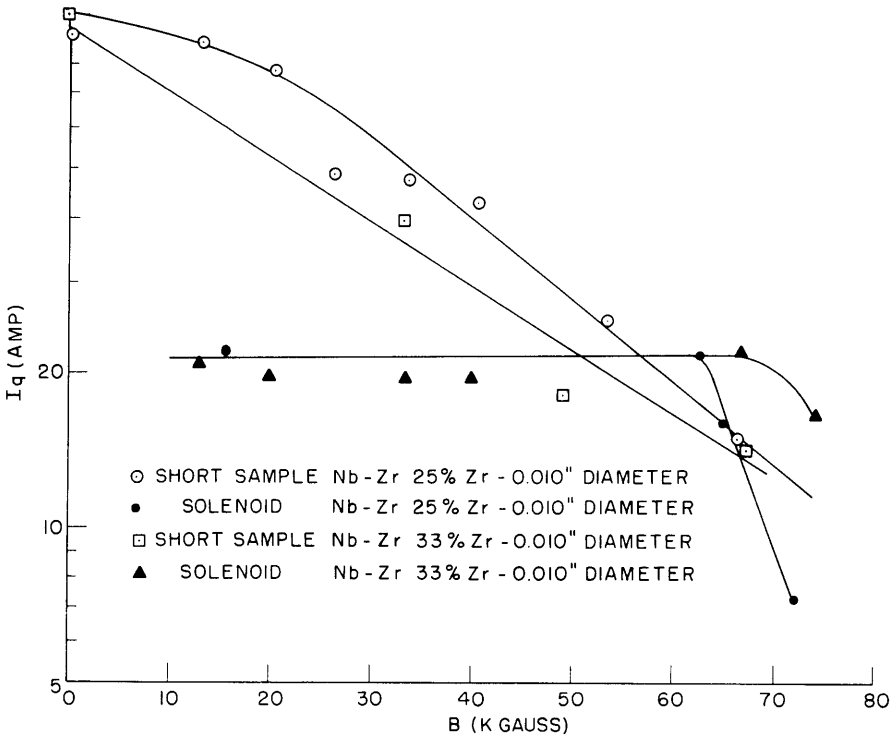

Fig. XV-18. Comparison of small solenoids and short samples.

What are the causes of such current limitations? Why do we have this magic value of 40,000 amps/cm^2, and can we increase the current density still more? These are questions to which we would like to know the answers.

A plausible cause is the length effect, since our short samples were between 2 ft and 13 ft long, and our small solenoids' wiring was approximately 300 ft long. We have not found any difference between 2-ft and 13-ft samples, and therefore there is no clear indication that the length is the actual cause, although it is highly suspected.

Other causes that may be involved are: (a) proximity of the other turns; (b) field gradient; (c) elastic deformations caused by the magnetic stress; (d) inhomogeneity of the wire; and (e) heat transfer.

No one cause can be ruled out certainly, although recent experiments at Lincoln Laboratory on the proximity effect have been negative.[13] Also, our experiment that was discussed in section (c) seems to rule out the heat-transfer effect.

We hope that heat treatment will raise the current density somewhat above the fatidic value, 40,000 amps/cm^2.

L. J. Donadieu

References

1. J. E. Kunzler, Paper V3, Bull. Am. Phys. Soc. II, 6, 298 (1961).

2. D. J. Rose and L. J. Donadieu, Quarterly Progress Report No. 62, Research Laboratory of Electronics, M.I.T., July 15, 1961, p. 68.

3. L. J. Donadieu and D. J. Rose, Paper K4, International Conference on High Magnetic Fields, Massachusetts Institute of Technology, November 1-4, 1961.

4. J. Wulff, Department of Metallurgy, M.I.T. (private communication).

5. Dr. J. Wong, Wah Chang Corporation, Albany, Oregon (private communication).

6. L. C. Salter, Jr., S. H. Autler, H. Kolm, D. J. Rose, and K. Gouen, Paper K13, International Conference on High Magnetic Fields, M.I.T., November 1-4, 1961.

7. Dr. J. Wong, Wah Chang Corporation, Albany, Oregon (private communication).

8. S. H. Autler, Lincoln Laboratory, M.I.T. (private communication).

9. L. J. Donadieu and S. H. Autler, Quarterly Progress Report No. 59, Research Laboratory of Electronics, M.I.T., October 15, 1960, pp. 27-30.

10. R. J. Triuteng, J. H. Warnick, and H. S. L. Hsu, Paper K6, International Conference on High Magnetic Fields, M.I.T., November 1-4, 1961.

11. J. D. Knight, J. O. Betterton, D. S. Easton, and J. O. Scarborough, Paper K10, International Conference on High Magnetic Fields, M.I.T., November 1-4, 1961.

12. L. J. Donadieu (unpublished results).

13. S. H. Autler, Lincoln Laboratory, M.I.T. (private communication).

K. NEUTRAL PARTICLE BURNOUT BY MOLECULAR ION INJECTION INTO A MAGNETIC MIRROR

A calculation is being made on the benefit to be expected from injecting a molecular ion beam into a magnetic mirror and trapping it there for a relatively long time. For example, if a helical magnetic field ("Corkscrew") is used for injection, it is estimated that 500 transits of a molecular ion may be obtained before the particle is lost by an accumulation of small nonadiabatic perturbations.

If the molecular ions are well contained, most of them will either dissociate to give atomic ions (which are subsequently lost only by coulomb collisions or charge transfer) or aid in the burnout of neutral gas (by charge transfer and/or direct ionization).

The calculations will not be given here. They are basically similar to those of Simon[1] and Mackin.[2] A summary of the general method has been given by Rose and Clark.[3]

For purposes of comparison, we took as parameters a molecular $\left(H_2^+\right)$ ion energy of

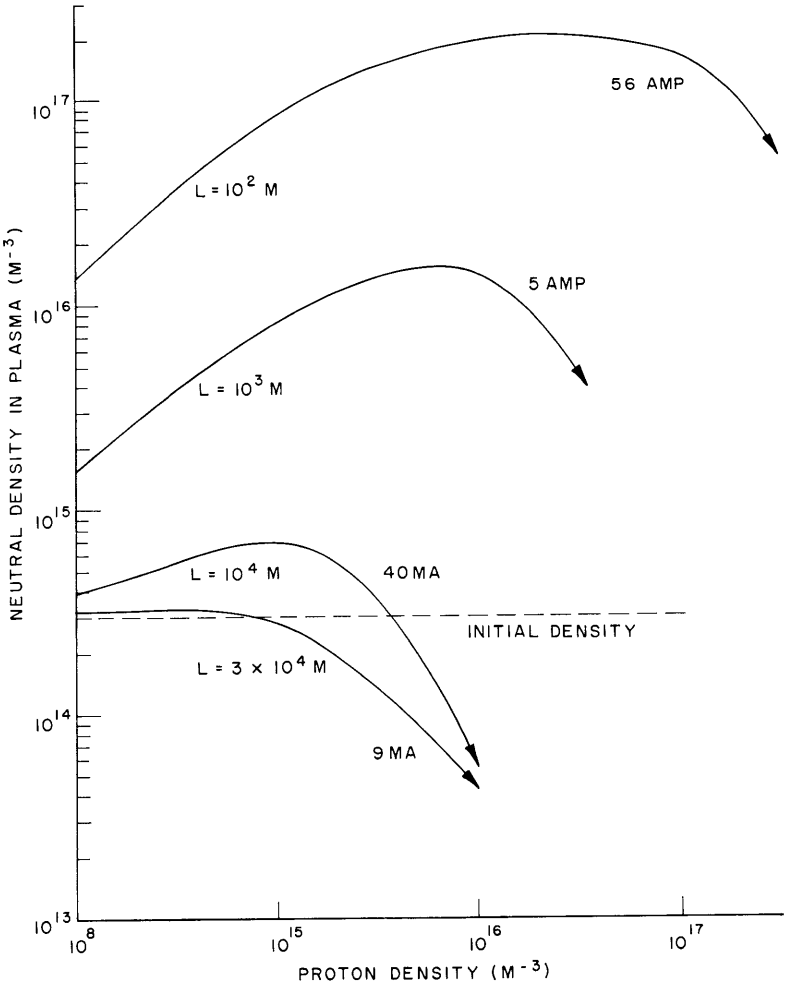

Fig. XV-19. Results of calculations.

100 kev, volume 1 m^3, pump speed 100 m^3/sec, and probability of gas return from the mirror throats 0.3. Interaction of slow ions (formed by charge transfer or ionization) with the fast plasma ions was neglected. It turned out to be convenient to solve for the neutral particle density in terms of the fast dissociated (atomic) ion density. Figure XV-19 shows the results for a base pressure of 10^{-8} mm Hg.

Injected molecular ion current is a running parameter along each curve. As the ion density rises, the neutral density rises more or less as the ion beam is dissociated, splashing neutral atoms about the vacuum region. The point of interest is the effect of the track length L of the molecular ions upon the neutral density, and upon the ion current required. For example, for a track length L = 100 m, representing a few molecular ion transits before the loss of ions, the situation is very bad, as we expected. The maximum current occurs at approximately the point shown (56 amps). The case L = 10^3 m gives 5 amps. The long-time molecular ion trapping is exemplified by the two lower

curves; $L = 3 \times 10^4$ m represents to some 500 transits. Even at this unfavorable energy of 100 kev for plasma production by this scheme, the maximum current is only approximately 9 ma.

Much more detailed calculations of these effects are being continued.

D. J. Rose

References

1. A. Simon, Phys. Fluids 1, 495 (1958).

2. R. J. Mackin, Nuclear Fusion 1, 131 (1961).

3. D. J. Rose and M. Clark, Jr., Plasmas and Controlled Fusion (The M.I.T. Press, Cambridge, Mass., and John Wiley and Sons, Inc., New York, 1961).

L. ENERGY EXTRACTION BLANKET FOR A FUSION REACTOR

This report is an extension of our discussion of the possibility of energy recovery from a hypothetical fusion reactor, which was begun in Quarterly Progress Report No. 62 (pages 64-68). The energy incident on the vacuum wall surrounding the plasma is assumed to consist of 14.2 Mev neutrons from the D(T, n) He^4 reaction, plus cyclotron radiation and bremsstrahlung from the plasma. Charged particles from the plasma do not strike the wall, but are guided out of the plasma (e.g., the mirrors for a mirror type of device) by some innocuous path. (It can be shown that if plasma material losses are to the hot vacuum wall, little chance exists for long-time structural integrity.)

Here, we consider the neutron transmission, neutron slowing down, and neutron multiplication, and the problems of heat transfer and tritium recovery in several sections of the proposed blanket assembly.

a. Material Considerations

If a mixture of fused lithium and beryllium fluoride is to be used both as a coolant and as a lithium bearer, the optimum molar ratio of Be:Li is approximately 34:66. The melting point of this mixture is 455°C. If the percentage of beryllium is lowered, the melting point increases sharply, and thus the usable temperature range between the melting point and a corrosion-determined upper limit of approximately 620°C is narrowed. If the beryllium content is raised, the viscosity of the mixture increases rapidly, with adverse effect on heat transfer and coolant pressure drop.

Comparison of this coolant with three other fused-fluoride coolants (by mole per cent, 57NaF:43BeF_2; 46.5LiF:11NaF:42KF, and 47ZrF_4:53NaF) at 500°C has shown its heat transfer properties to be most favorable. It has thus been used as the first-wall coolant in preliminary neutronics and heating calculations.

Little difficulty is anticipated in removing tritium from a $LiF\text{-}BeF_2$ mixture. Hydrogen and HF are very slightly soluble in the fused-fluoride mixture, and can easily be removed continuously by sparging with helium at the circulation pumps.[5] Tritium and TF should behave quite similarly, and can be readily separated from helium by chemical methods or by fractional distillation. It will be necessary to keep the tritium concentration low to prevent corrosion by $TF\left(xH^3F + M \rightarrow MF_x + \frac{x}{2} H_2^3\right)$. The presence of a small concentration of beryllium in the fused-fluoride mixture will probably prevent corrosion by fluorine formed in the nuclear chemical reaction $BeF_2 + n \rightarrow 2n + 2He + F_2$. There are no experimental data on this question or on the solubility of Be in $LiF\text{-}BeF_2$. Lithium is known to be highly soluble and would be a possible substitute. The corrosion effects of oxygen formed by the nuclear reactions $F^{19} + n \rightarrow He^4 + N^{16} \rightarrow He^4 + O^{16} + \beta^-$ ($\sigma \sim 150$ mb $4 < E_n < 14$ Mev) and $F^{19} + n \rightarrow 2n + F^{18} \rightarrow 2n + \beta^+ + O^{18}$ ($\sigma = 62$ mb for $E_n = 14.1$ Mev) have yet to be studied.

Although strong magnetic fields and field gradients have been found to have negligible effects on chemical processes,[3] induced electric fields cannot be neglected. To prevent rapid voltage-increased corrosion of container walls, either fluid velocities perpendicular to the magnetic field, or duct widths mutually perpendicular to the magnetic field and fluid, may have to be limited.

Molybdenum was selected as the first-wall material for preliminary studies, because of its refractory properties and its superiority to tungsten in fabricability. Cladding of the coolant side with INOR-8, a nickel-molybdenum alloy developed to resist fused salts, will be necessary to prevent corrosion. INOR-8 and molybdenum can be joined by brazing.

b. Neutronic Calculations

Recent efforts relating to neutron economy problems have been directed primarily toward calculation of the neutron flux distributions in the so-called first region of the blanket assembly. This region is expected to consist of a first wall a few centimeters thick, a first-wall coolant channel, perhaps, 5 cm deep, and a back-up region, approximately 20 cm thick, and is intended to provide first-wall cooling, neutron multiplication, and neutron primary slowing down.

A digital computer code in IBM FORTRAN II language has been developed to expedite calculation of the flux distributions on the basis of rather straightforward transport theory. The code is designed to carry out calculations of the flux distributions in a total of 34 lethargy groups spanning the range from 14.2 Mev to 400 kev. The system configuration consists of three homogeneous subregions corresponding to the first wall, the coolant channel, and the back-up region, respectively, in slab, cylindrical, and spherical geometries. At present, the code is operational in the slab option for all source distributions, and is in the final stage of debugging in the cylindrical and spherical options.

Simultaneously, a program is being carried on to develop a cross-section library, tailored to the requirements of the code, for the various nuclides of potential interest in the several blanket configurations that are to be considered.

A sample problem has been run in the code for the slab option. The configuration consisted of 3 cm of molybdenum, 5 cm of 31 per cent BeF_2-69 per cent LiF, and 20 cm of a homogeneous mixture of equal volumes of molybdenum and the fused salt. A cosine source distribution of plasma-born neutrons, equivalent to that expected from a long mirror machine with a plasma radius to inner-wall radius ratio of approximately 2/3, was assumed at the first surface.

The computer calculations indicate that for each source neutron incident on the first wall, approximately 0.09 neutron emerges from the back-up wall with energies above 400 kev, while 0.95 neutron is degraded in energy below 400 kev in the first region. Since calculations reported previously[4] have shown that essentially all neutrons entering the second region are slowed down below 400 kev without absorption, a net yield of approximately 1.04 epithermal neutrons per source neutron is predicted for this geometry.

An interesting side light arising from the cross-section investigations, together with these flux distributions, is the prediction that approximately 0.02 neutron per source neutron will undergo reactions of the general form

$$Li^7 + n \rightarrow n + H^3 + He^4$$

in the configuration noted above. Reactions of this type are in effect neutron-multiplying reactions, since the net yield of the reactions is a triton plus an additional neutron. With this contribution included, the net yield in the sample configuration investigated is calculated to be approximately 1.06 neutrons per source neutron.

Multiplications as small as that calculated for this configuration are almost certainly too small to permit one-for-one tritium regeneration. However, the neutron yield can be increased in several ways. Increasing the first-wall thickness will yield a corresponding increase in the number of (n, 2n) reactions that take place before the neutrons are elastically degraded in the fused salt. Decreasing the coolant channel width will allow more fast neutrons to reach the back-up region and cause (n, 2n) reactions there. Alternatively, the use of heavy fused salts based on lead and/or cesium in the primary coolant channel would both increase the (n, 2n) probability and decrease degradation of energy arising from elastic scattering. Introduction of additional beryllium in the back-up region will also yield an increase in the (n, 2n) contribution caused by neutrons partially slowed down by elastic collisions in the fused salt, since the (n, 2n) threshold in beryllium is much lower than that in the heavy elements such as molybdenum.

c. Heat Transfer

The feasibility of the first three schemes suggested above depends on the heat loads on the first wall and consequent cooling difficulty. A first approximation to first-wall heating was calculated for a high energy density (Stellarator 75 kgauss) device and the blanket composition that has been described here. We assumed that all nonelastic reactions deposit their gamma energy in the first wall. The heat liberated in the first wall, excluding cyclotron radiation and bremsstrahlung heating, was 3.6 Mw/m^2. The pump work required to cool the first wall was 0.25 per cent of the heat transferred through the wall, under the assumption that there was 1 Mw/m^2 of cyclotron radiation and bremsstrahlung heating, a bulk coolant temperature of 500°C, and a coolant-wall interface temperature of 620°C. An increase in the heat load of 1 Mw/m^2 raises the pump work to 0.4 per cent of the total heat transfer. The coolant temperature rise per meter of travel along the wall is 2.3°C/meter.

Increasing the wall thickness, narrowing the coolant channel or changing the coolant salt thus, to some extent, are compatible with heat-transfer limitations. The last of these will also depend on corrosion properties that have not been discussed in published work.

These heating estimates are probably conservative because gamma transport has been neglected. As more neutronics data are produced by the computer, gamma-heating calculations will be made by an integral spectrum method[2] with "energy absorption coefficients"[1] used to allow for build-up. In this approximation it is assumed that photon scatterings are all straight ahead and that the gamma spectrum remains constant. Molybdenum can be expected to produce a spectrum that is well distributed between 0 and 3 Mev as a result of de-excitation of its seven stable isotopes and three unstable reaction products.

The concentric annuli of blanket materials will be approximated by infinite slabs. The radii of curvature of practical systems are more than one order of magnitude greater than the gamma mean-free paths.

W. G. Homeyer, A. J. Impink, Jr.

References

1. L. G. Alexander, The Gamma Energy-Absorption Coefficients, Report (CF56-8-219), Oak Ridge National Laboratories, Oak Ridge, Tennessee, August 8, 1956.

2. L. G. Alexander, The Integral Spectrum Method for Gamma Heating Calculations in Nuclear Reactors, Report (CF56-11-82), Oak Ridge National Laboratories, Oak Ridge, Tennessee, November 21, 1956.

3. F. W. Camp and E. F. Johnson, The Effect of Strong Magnetic Fields on Chemical Engineering Systems, Report MATT-67, Project Matterhorn, Princeton, New Jersey, March 1961.

4. W. G. Homeyer, A. Impink, Jr., D. J. Rose, and I. Kaplan, The fusion reactor blanket problem, Quarterly Progress Report No. 62, Research Laboratory of Electronics, M.I.T., July 15, 1961, pp. 64-68.

5. R. A. Strehlow, Oak Ridge National Laboratories (Personal communication, November 20, 1961).